Naval Research Laboratory
Washington, DC 20375-5320

NRL/FR/7127--93-9580

Measurements and Modeling of Multitone, Low-Frequency Acoustic Data from the Arraial do Cobo Range

WILLIAM SOARES-FILHO
JOSÉ ROBERTO MOTTA DA SILVA

Instituto de Pesquisas da Marinha
Rio de Janeiro, R.J., Brazil

STEPHEN N. WOLF

Acoustic Signal Processing Branch
Acoustics Division

October 15, 1993

Approved for public release; distribution unlimited.

REPORT DOCUMENTATION PAGE

Form Approved
OMB No. 0704-0188

1. AGENCY USE ONLY (*Leave Blank*)	2. REPORT DATE	3. REPORT TYPE AND DATES COVERED
	October 15, 1993	Final

4. TITLE AND SUBTITLE

Measurements and Modeling of Multitone, Low-frequency Acoustic Data from the Arraial do Cabo Range

5. FUNDING NUMBERS

PE 0602435

6. AUTHOR(S)

William Soares-Filho, José Roberto Motta da Silva, and Stephen N. Wolf

7. PERFORMING ORGANIZATION NAME(S) AND ADDRESS(ES)

Naval Research Laboratory
Washington, DC 20375-5320

8. PERFORMING ORGANIZATION REPORT NUMBER

NRL/FR/7127--93-9580

9. SPONSORING/MONITORING AGENCY NAME(S) AND ADDRESS(ES)

Office of Naval Research
800 North Quincy Street
Arlington, VA 22217-5660

10. SPONSORING/MONITORING AGENCY REPORT NUMBER

11. SUPPLEMENTARY NOTES

Prepared in collaboration with the Instituto de Pesquisas da Marinha, Rio De Janeiro, R.J., Brazil

12a. DISTRIBUTION/AVAILABILITY STATEMENT

Approved for public release; distribution unlimited.

12b. DISTRIBUTION CODE

13. ABSTRACT (*Maximum 200 words*)

A study was performed to characterize short-range, low-frequency acoustic propagation at the Arraial do Cabo acoustic range, which is located in shallow water on the Southeast coast of Brazil. Acoustic transmission data, obtained by using multitone continuous-wave (CW) transmissions from uncalibrated sound sources and omnidirectional receivers were compared with predictions of normal-mode acoustic transmission models. The measurements, which were made along the 17- and 47-m isobaths, extended over the frequency range from 12 to 375 Hz. It was found that, for most of the data, short-range multipath interference patterns were in agreement with results calculated by modeling the ocean bottom as a fluid. At frequencies below 80 Hz, the influence of shear waves in the ocean bottom was found to be important for the data taken in water depth 17 m. Recommendations are made to help guide follow-on modeling and experimental acoustic propagation studies.

14. SUBJECT TERMS

Shallow water acoustic measurements
Low frequency underwater acoustic propagation
Acoustic measurement range
Acoustic modeling

15. NUMBER OF PAGES

36

16. PRICE CODE

17. SECURITY CLASSIFICATION OF REPORT	18. SECURITY CLASSIFICATION OF THIS PAGE	19. SECURITY CLASSIFICATION OF ABSTRACT	20. LIMITATION OF ABSTRACT
UNCLASSIFIED	UNCLASSIFIED	UNCLASSIFIED	UL

CONTENTS

MEASUREMENTS AND MODELING OF MULTITONE, LOW-FREQUENCY ACOUSTIC DATA FROM THE ARRAIAL DO CABO RANGE

INTRODUCTION

The Brazilian Navy has an acoustic range on the southeastern Brazilian coast at Arraial do Cabo in the Rio de Janeiro state, 180 km east of Rio de Janeiro city (Fig. 1). This range is operated by CASOP (Operative Systems Analysis Center) and is used to measure radiated noise emitted by ships and submarines and to test acoustic and oceanographic equipment. These measurements are normally performed in a frequency range from a few Hz up to tens of kHz and with typical source-to-hydrophone distances up to 2 km. Acoustic calibration and modeling of the range are required for accurate analysis and interpretation of the radiated noise measurements.

This report gives the results of a preliminary study of the low-frequency (up to 375 Hz) characteristics of sound propagation at the acoustic range. The study was performed by analyzing some data recorded previously during source tests. The purpose of the study is to guide future work aimed at a more thorough acoustic environmental characterization of the Arraial do Cabo site.

THEORETICAL ASPECTS

At the low acoustic frequencies of interest in this study, the propagation of sound in shallow water is conveniently described by normal-mode theory. For a range-independent environment, as is considered here, the environment is usually modeled as a stratified medium in which a number of fluid layers, which represent the water and sediment, overlie a halfspace, which represents the geological basement. In the normal-mode representation of a range-independent acoustic environment, the sound field produced by projecting a continuous-wave (CW) acoustic signal is represented as a sum of terms, each of which is associated with a single normal mode of propagation [1, Chapters 2-4]. If the sound source has rms source pressure S, referred to unit distance from the source, then the pressure $p(r,z)$ at depth z and range r from the source located at depth z_s is:

$$p(r,z) = (4\pi)^{1/2} S\rho \sum_{n=1}^{N} \frac{u_n(z_s)u_n(z)^{1/2}}{k_n r} e^{ik_n r - \delta_n r}. \quad (1)$$

The density of the water is represented by ρ. The normal-mode depth function of the nth mode is u_n, and the wave number and attenuation coefficients of the nth mode are represented by k_n and δ_n, respectively. The relative amplitudes of these normal-mode components depend on the product of the depth-dependent normal-mode amplitude function at the source and at the receiver as well as on the attenuation of the modal component because of absorptive losses in the medium. If more than one normal-mode component is present, then range-dependent interferences are observed, because of the range-dependent phase differences of the modal signal components. These phase differences are due to the mode-order dependence of the horizontal component of the wave number k_n. The interference distance Λ_{nm} between the nth and mth modal component is given by the expression,

$$\Lambda_{nm} = 2\pi(k_n - k_m)^{-1}. \quad (2)$$

Manuscript approved July 7, 1993.

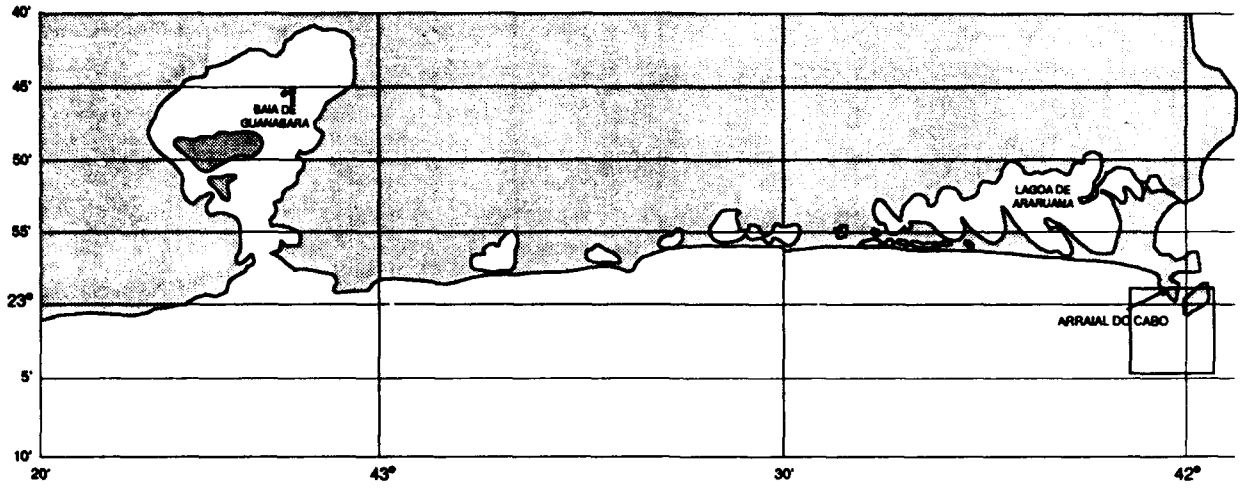

(a)

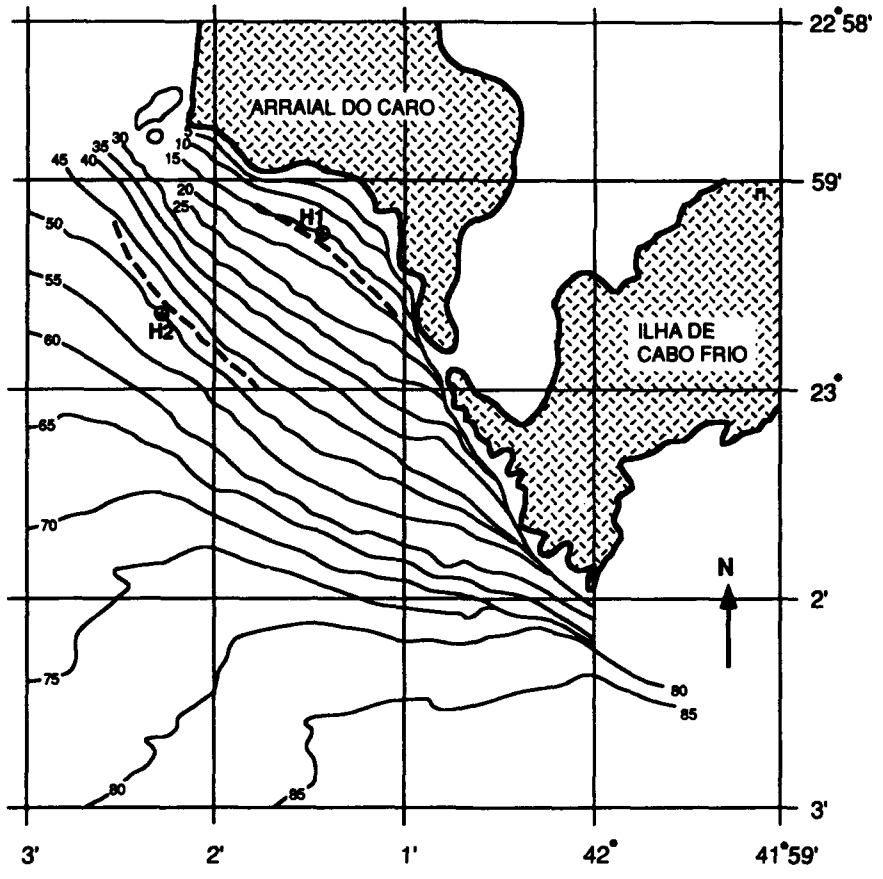

(b)

Fig. 1 — (a) Location of the Arraial do Cabo site, and (b) expanded bathymetric chart of the Arraial do Cabo site showing tow tracks (dashed lines) and the hydrophone locations (H1 and H2)

The wave number of the nth modal component is related to the component's phase speed c_n by the expression,

$$k_n = \omega/c_n. \tag{3}$$

Here ω is the angular frequency $2\pi f$, where f is the harmonic frequency of the signal. For a given signal frequency, the specific values of the wave numbers associated with the normal modes are determined by solving the depth-dependent portion of the wave equation, subject to the appropriate boundary conditions. These wave numbers vary over a range of values determined by the range of sound speeds in the acoustic environment. For an environment that is modeled as a number of fluid layers overlying a uniform halfspace, the modal phase speeds will lie between the bounds of the lowest compressional sound speed in the profile and the highest compressional sound speed, which is usually the compressional sound speed in the lower halfspace. If the sediment layer or the halfspace is permitted to support shear, then the range of speeds over which the modal phase speed varies is increased. For a given geophysical model, as the acoustic frequency is increased, the spatial frequency range (range of k_n) increases in direct proportion to the harmonic frequency, since the range of values of c_n is fixed. Thus for a given range of phase speeds, we expect the spatial interference pattern of a CW signal to show a structure that increases in complexity as the frequency is increased.

EXPERIMENTAL

The data used in this report were obtained in a test performed in March, 1985. The original purpose was to test some sound sources which had motor-driven pistons. Two types of acoustic sources were used. The first type, which used a cam to directly drive a piston, was effective in producing low-frequency signals. The other source operated by striking a resonant plate with a motor driven piston and was more efficient at higher frequencies. These sources are referred to as the low-frequency and high-frequency sound sources, respectively.

In most of the runs, the rotational speed of the motor that drove the sound sources' pistons was varied constantly, with the result that the frequencies of the acoustic signals emitted by the source changed during the run. In some of the runs, the rotational speed was held constant or nearly so. These stable-frequency runs were selected because the data were useful to study the range-dependent interferences of the signal components. Since the sound sources used in this test did not have calibrated source levels, absolute transmission loss could not be measured, and an alternate method of verifying the reasonableness of the specification of the acoustic environment needed to be found. We use agreement of the measured and modeled spatial interference patterns of the CW signals as an indication that the geoacoustic environment is correctly specified.

The operation of the two types of sound sources used is described in Appendix A. The acoustic waveform produced by the sources is not sinusoidal, with the result that the signal emitted is rich in harmonics of the drive frequency. This circumstance permits the investigation of acoustic propagation at several frequencies with each source tow. Unlike propagation studies often seen in literature, this study deals with short ranges (less than 800 m) over a broad range of low-acoustic frequencies (12 to 375 Hz).

The water depths at the acoustic range vary from 15 to 50 m. The acoustic data chosen for analysis were obtained on tracks extending radially from the receiver along the 17- and 47-m isobaths. Data from tow tracks along isobaths were chosen so that comparisons of the observed interference patterns as a function of range could be made with predictions of a simple range-independent normal-mode model. This comparison is made more complex if the wave number differences of the modal components are themselves range-dependent, as would be the case if water depth varied over the propagation track. The ratio of the acoustic wavelength λ to the water depth H_1 varies from large values $\lambda/H_1 \sim 7$ for the

low-frequency signals at the shallow site (for 12 Hz and c = 1500 m/s, λ = 125 m) down to a value of about 0.1 for the high-frequency signals at the deeper water site (using 375 Hz and c = 1500 m/s, λ = 4 m). Thus one can expect that the character of the bottom interaction that controls propagation will be different for the low- and high-frequency regimes of these data.

Experimental Procedures

In all cases the sources were towed by a ship as shown in Fig. 2(a). A float was used to maintain a constant source depth of about 6 m. In the runs considered here, the tow ship ran along either the 17- or 47-m isobath at a speed of about 6 knots (~3 m/s). Navigation data used for precision measurements of range from the receiver were obtained by triangulation using two shore-based theodolites, with the source position obtained at 30-s intervals throughout each run.

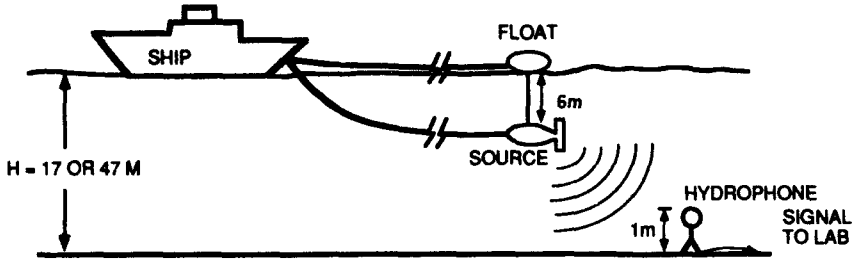

(a)

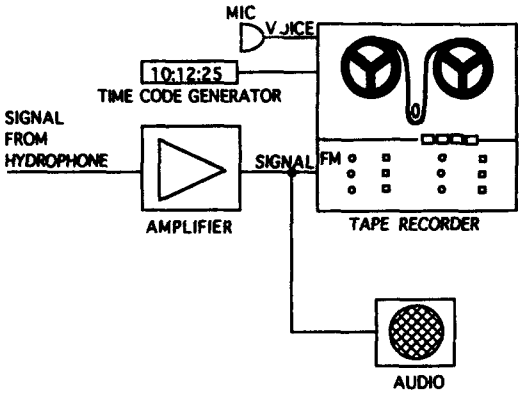

(b)

Fig. 2 — (a) Experimental configuration (b) Signal recording equipment

The data studied here were obtained from two hydrophones positioned 1 m above the bottom. One was located at the 17-m isobath; the other at the 47-m isobath at locations shown in Fig. 1(b). The received signals were sent via cable to a building on the shore, where they were conditioned (filtered and amplified) and recorded along with time code and voice annotation (Fig. 2(b)). The acoustic signals were recorded during the inbound and outbound runs, when the source was within 800 m of the closest point of approach (CPA) to the hydrophones. Table 1 shows speed and CPA (in plan view) to the receiver for the runs used in this study.

ACOUSTIC ENVIRONMENT

The original purpose of this test was not to study acoustic propagation, but rather to test the acoustic sources. For this reason, ocean acoustic environmental measurements were not made at the time the test

Table 1 — Navigational Data

Run #	Water Depth (m)	Ship Speed (m/s)	CPA (m)
01	47	3.56	1
02	17	2.78	30
06	17	2.57	22
07	47	2.88	44
12	17	3.56	23

was performed. The information about the environment in the acoustic range presented here is limited to that available to the authors from archival sources.

The water temperature profile was not measured during the experiment. However, temperature profile information taken at the acoustic range during March 1974 was available. Figure 3 shows sound speed profiles calculated from the archival temperature data. Only the first of these profiles Fig. 3(a) was used in the models during this study. We note that the profiles have been observed to depend on wind direction, with the prevailing profile depending strongly on the presence or absence of the upwelling phenomenon accompanying offshore winds common in that region in some periods of the year.

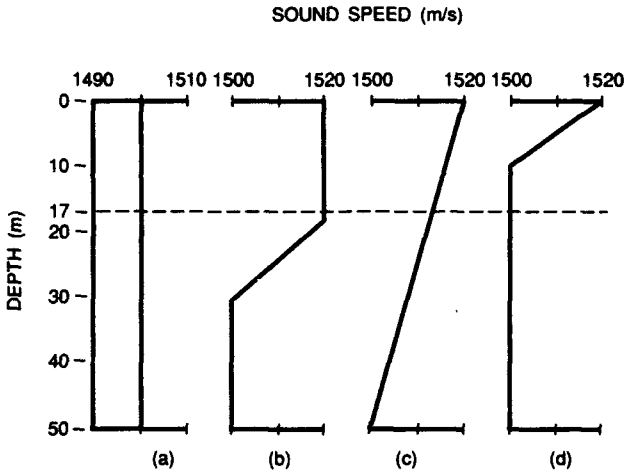

Fig. 3 — Representative water sound speed profiles for the months of March, taken from archival sources

No bottom sediment study was made at the range location, so the descriptions used were based on the observations of one of the authors (W.S.-F) that the ocean bottom in the area is composed mainly of fine sand. This description agrees with reports made by divers about weights on the sea floor being covered with sand some time after deployment. This agrees, too, with Ref. 2, which describes sand in sample cores taken during a propagation experiment 100 miles west of the acoustic range. However, contradictory information is given by an oceanographic chart [3] produced by the Brazilian Navy Directorate of Hydrography and Navigation (DHN), which shows that region's bottom composed mainly of mud. The authors regarded the oceanographic chart as being less reliable, so the parameters used in the modeling were based on an assumed sandy bottom. This choice appears to be justified by the agreement of the modeled results with the measurements.

Additional environmental information is available from the Brazilian Navy IEAPM (Institute for Sea Studies Admiral Paulo Moreira) and DHN. This information will be used in follow-on work.

RESULTS

Plots of the received pressure levels, displayed as a function of range from the receiver, showed variations that were due to two causes. The first was the expected cylindrical spreading trend in which the signal level (in dB) is reduced as 10 log R, where R is the horizontal range between source and receiver. This trend was usually the largest range-dependent trend in the data, so its influence was removed from both the measurements and calculations to make other range-dependent level variations easier to compare. Acoustic pressure level adjusted to remove the 10 log R trend will be referred to as "loss anomaly." The second range-dependent level variation was apparently due to the coherent interference of the multiple acoustic paths (multiple modes of propagation) between source and receiver.

Data Reproducibility

The analysis of the range-dependent acoustic pressure variations was begun by determining the degree to which the observed variations are reproducible and therefore attributable to deterministic causes appropriate for modeling analysis. Of the runs available for study, only runs 2 and 12 were considered to be sufficiently similar that comparison of the results would be indicative of data reproducibility. For these runs, the low-frequency source was towed at 6 m along the 17-m isobath and was driven to provide a 12 Hz (fundamental frequency) signal. Both closing and opening range (i.e., approaching and receding from the receiver, respectively) data were available for these two runs, which were conducted six days apart. Both runs were made with the ship's tow track running from northwest to southeast, so both closing range tracks were run over nominally the same ground, as were the opening range runs. Figures 4 through 7 show some of the data comparisons made (using loss anomaly referred to an arbitrary reference).

Figure 4 shows a comparison of the 12 Hz signal level vs range for the two opening-range runs. Although the source frequency was the same for the two runs, different source levels were used. The piston amplitude for run 2 was 0.5 in.; for run 12 the amplitude was 0.125 in., suggesting a source level decrease of 12 dB (i.e., the volume velocity was reduced by a factor of 4 when the piston stroke was reduced by this factor). In overlaying the two signal-level-vs-range traces, the relative vertical positions were adjusted "by eye" to obtain the best overall agreement in level. The total adjustment made was 15 dB, close to the 12 dB expected from consideration of the change in piston amplitude. Locations of the interference maxima and minima at ranges less than 400 m are reproduced to an accuracy of about 10 m. Over most of the range interval the relative heights of the constructive interferences are reproduced to an accuracy of 1 or 2 dB; in the range interval 300 to 420 m, the relative heights differ by about 4 dB.

In Fig. 5 we compare the signal levels observed for the two runs on the closing range track. The data are found to agree in relative level and interference structure at ranges less than 350 m. Beyond that range the quality of the agreement, particularly the spatial frequency content, is poorer. In Fig. 6 we compare results from the inbound and outbound tracks for run 2. Similar spatial frequency content is observed, with interference nulls appearing about every 30 m at ranges less than 500 m, but the detailed agreement in the interference pattern, particularly for ranges less than 300 m, is somewhat poorer than was found in Figs. 4 and 5.

In Fig. 7 we compare the 24 Hz measurement results for the closing- and opening-range tracks in run 12. As expected, higher spatial interference frequencies are observed at 24 Hz than were seen at 12 Hz in Figs. 4 through 6. The 24 Hz data show "envelope" level agreement (ignoring discrepancies in the positions of the interference nulls) over much of the range interval and the coincidence of some interference features; however, there is disagreement of 5 to 10 dB in level over the range intervals 100 to 150 m and 400 to 450 m.

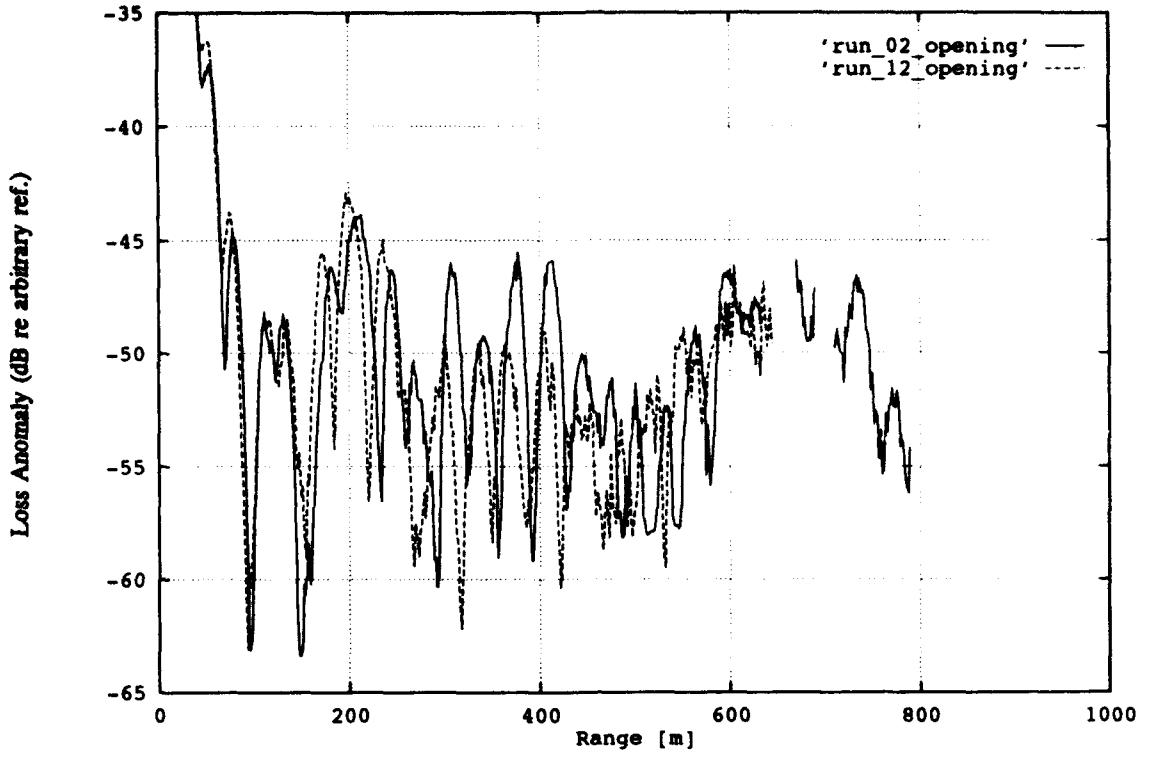

Fig. 4 — Comparison of CW loss anomaly vs range measurements at 12 Hz for opening-range runs 2 and 12 along the 17-m isobath

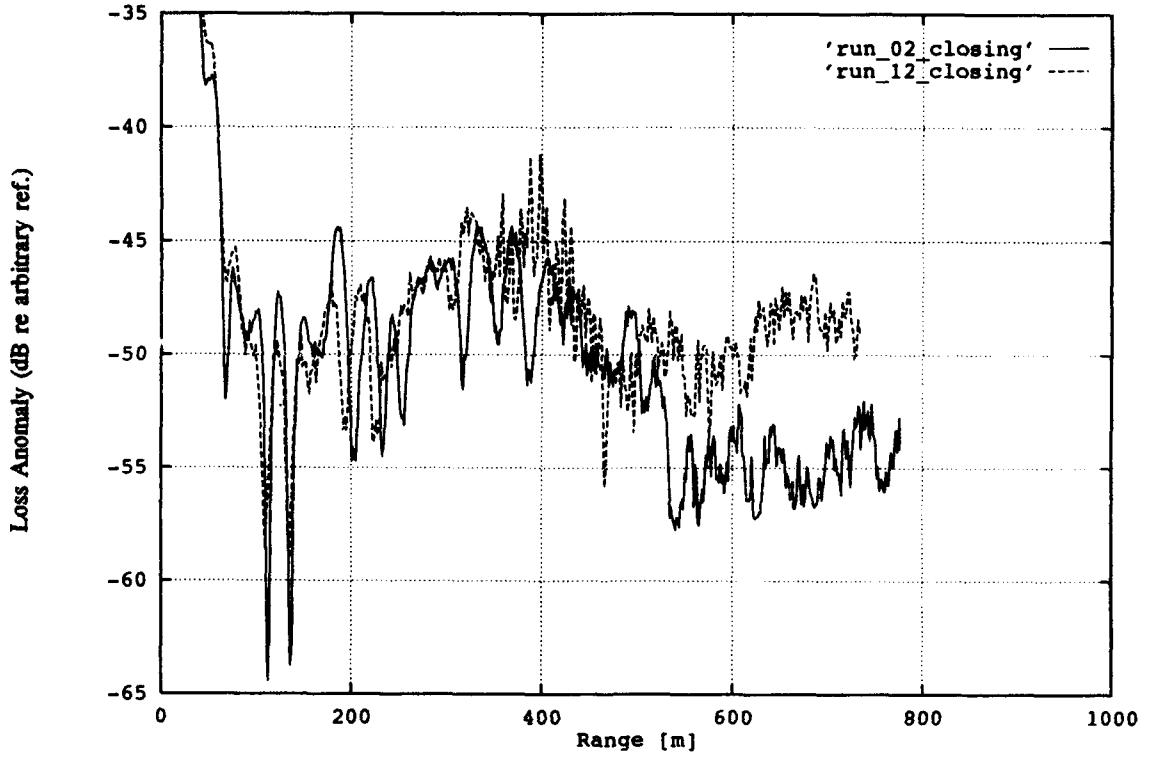

Fig. 5 — Comparison of CW loss anomaly vs range measurements at 12 Hz for closing-range runs 2 and 12 along the 17-m isobath

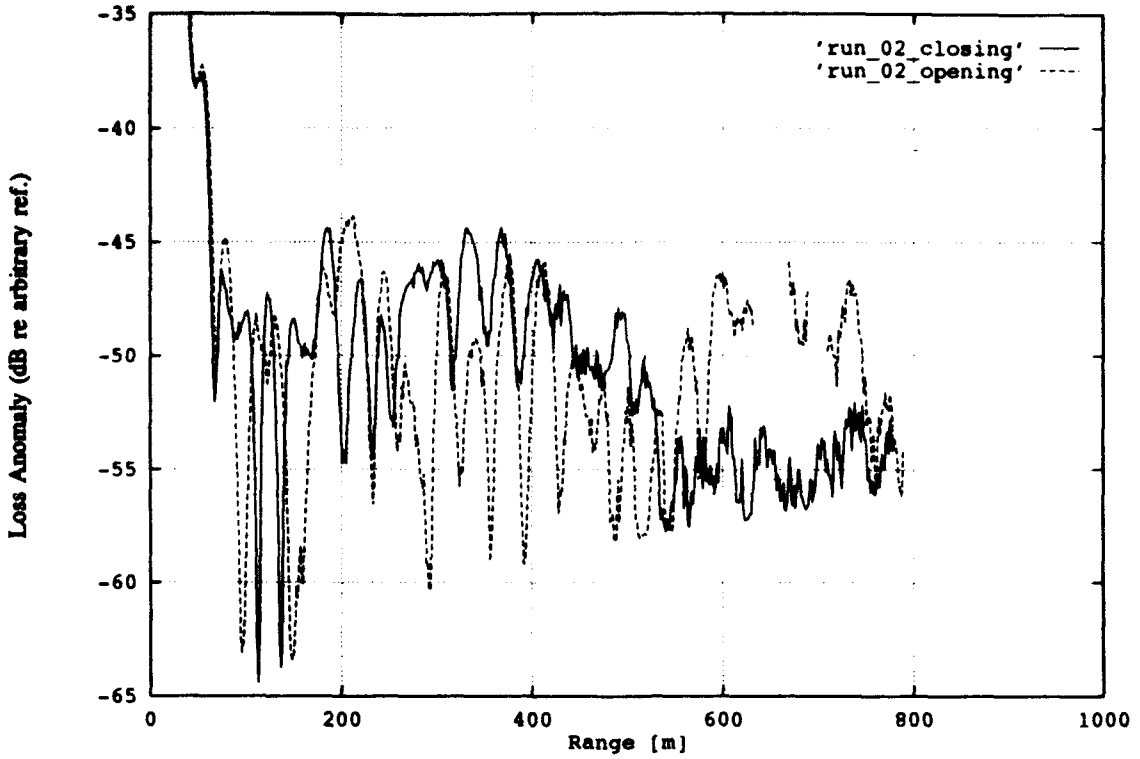

Fig. 6 — Comparison of CW loss anomaly vs range measurements at 12 Hz for the inbound and outbound tracks of run 2.

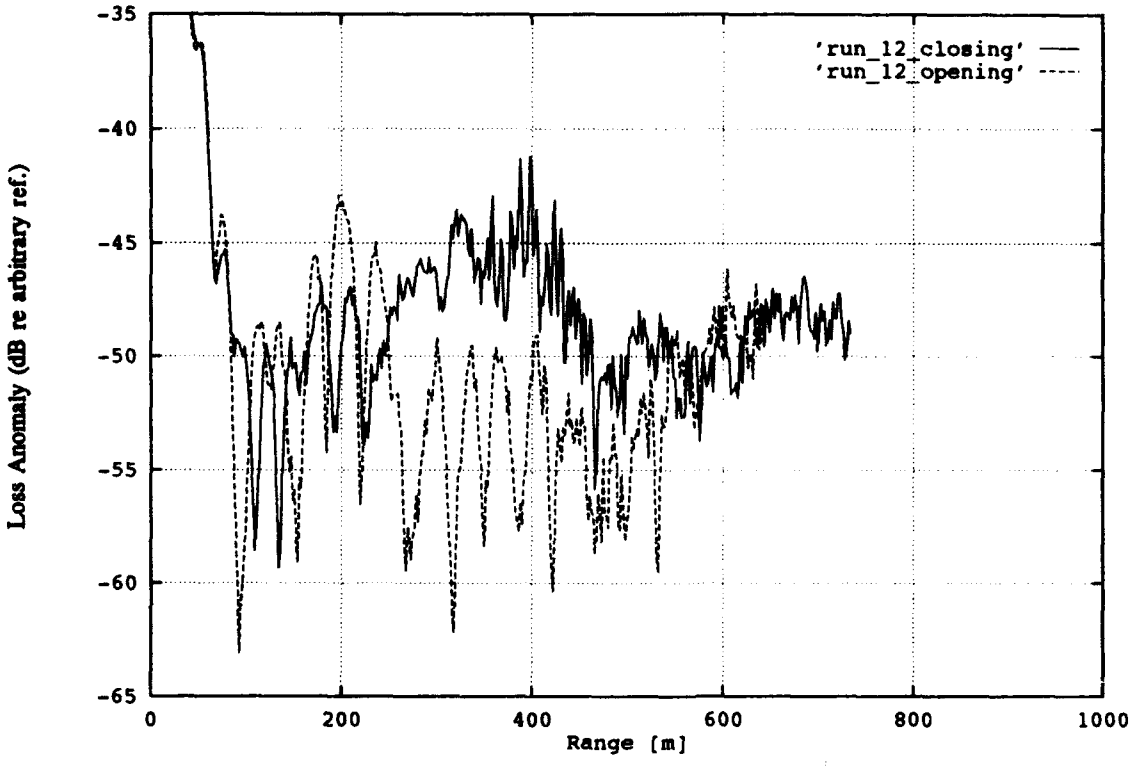

Fig. 7 — Comparison of CW loss anomaly vs range measurements at 24 Hz for the inbound and outbound tracks of run 12

From the comparisons shown in Figs. 4 through 7, we conclude that the spatial frequency content of the multipath interference pattern is reproducible, but the specific locations and depths of the nulls are not, particularly when comparison is made of the opening and closing range tracks. Better reproducibility of detail is made with runs over the same track, in spite of the six days' time difference in the acquisition of the data. This result suggests that there may be static (and at present unknown) environmental differences, such as variation in the sediment acoustical properties that occur over distances on the order of a few hundred meters. Thus we may reasonably expect that modeled transmission, which at best includes mean values of the sediment acoustical properties, will show no better agreement with measurements than is found in these data reproducibility comparisons.

Model-Data Comparisons

As discussed above, we use the transmission loss anomaly (i.e., transmission loss from which the cylindrical spreading trend is removed) to compare range trends of the data and model calculations. The reference level for the loss anomaly used in these plots is obtained from the model calculations. In adjusting the model parameters in the fluid normal-mode model [4,5] to fit the observed transmission loss anomaly, only the parameters that made significant differences in the loss, such as the sediment and bottom sound speeds and the sediment thickness, were varied. Details of the modeling procedures and investigations to determine the sensitive model input parameters are given in Appendix C. The best model fits were obtained at frequencies higher than 80 Hz. The fitting process began by adjusting the parameters for a good fit in these higher frequency data. When the model was applied to the lower frequency data, significant disagreements remained, and some features of the data could be fit better by further adjustment of the parameters. Table 2 shows the fluid-model parameters producing the best fits.

Table 2 — Values of Fluid-Model Environmental Parameters

Frequency (Hz)	Depth (m)	Run #	H_2 (m)	$C_{2P}(H_1)$ (m/s)	$C_{2P}(H_1 + H_2)$ (m/s)	C_{3P} (ms/s)
12	17	02	200	1630	1650	2000
24	17	12	100	1630	1640	4000
50	17	02	70	1630	1640	2000
80	17	06	100	1632	1642	2750
175	17	06	100	1632	1642	4000
375	17	06	100	1640	1650	2000
12	47	01	500	1630	1640	2000
24	47	01	100	1632	1642	4000
50	47	01	200	1630	1640	3500
80	47	07	100	1630	1640	2500

Other parameters used were: $C_{1P}(z) = 1500$ m/s; $\rho_1 = 1.0$ g/cm^3; $\rho_2 = 1.8\rho_1$; and $\rho_3 = 2.0\rho_1$.

17-m Water Depth

The modeled transmission loss anomaly at 80 Hz is compared with the measured data on the closing range track in Fig. 8(a) and with the opening range track in Fig. 8(b). Over most of the tracks, the spatial frequency structure of the data seems to be present in the model results, although in many cases the two results differ in the locations of the interference maxima and minima. Similar model-data agreement is found at 175 Hz in Fig. 9 and at 375 Hz in Fig. 10, although some significant and reproducible departures from the model results are seen in the 375 Hz data at ranges larger than 600 m. As expected, the spatial frequency content of the interference patterns increases as the acoustic frequency is increased.

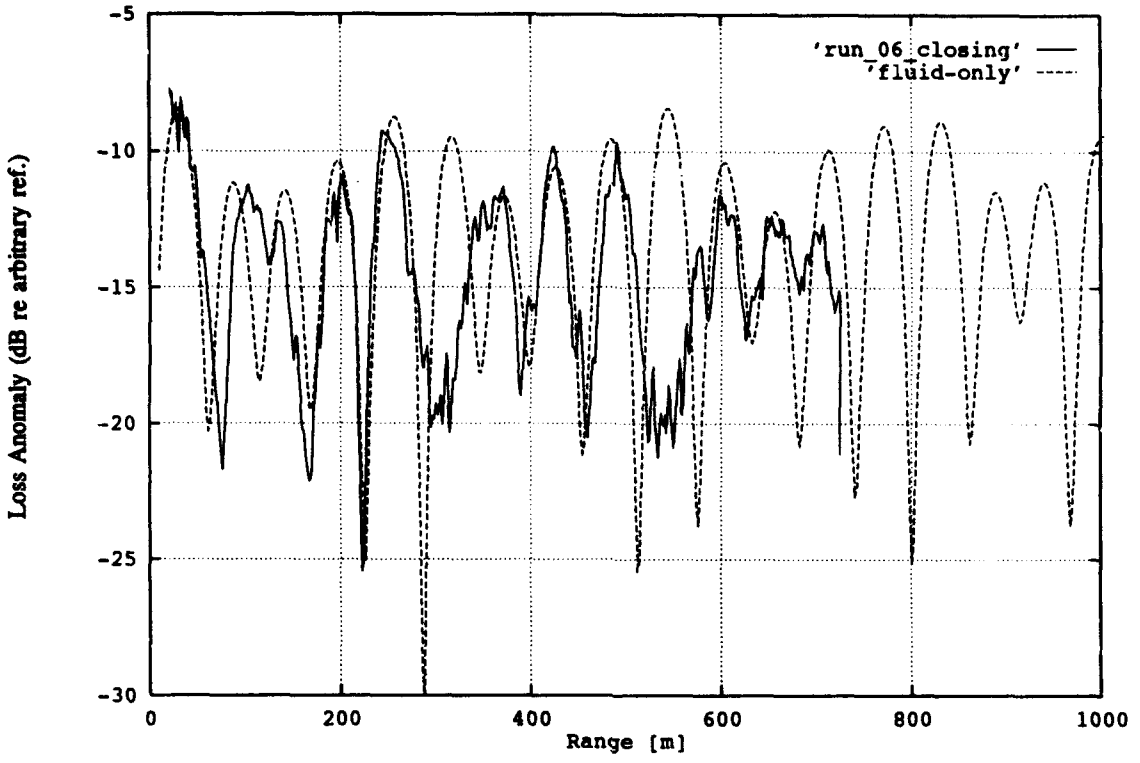

(a)

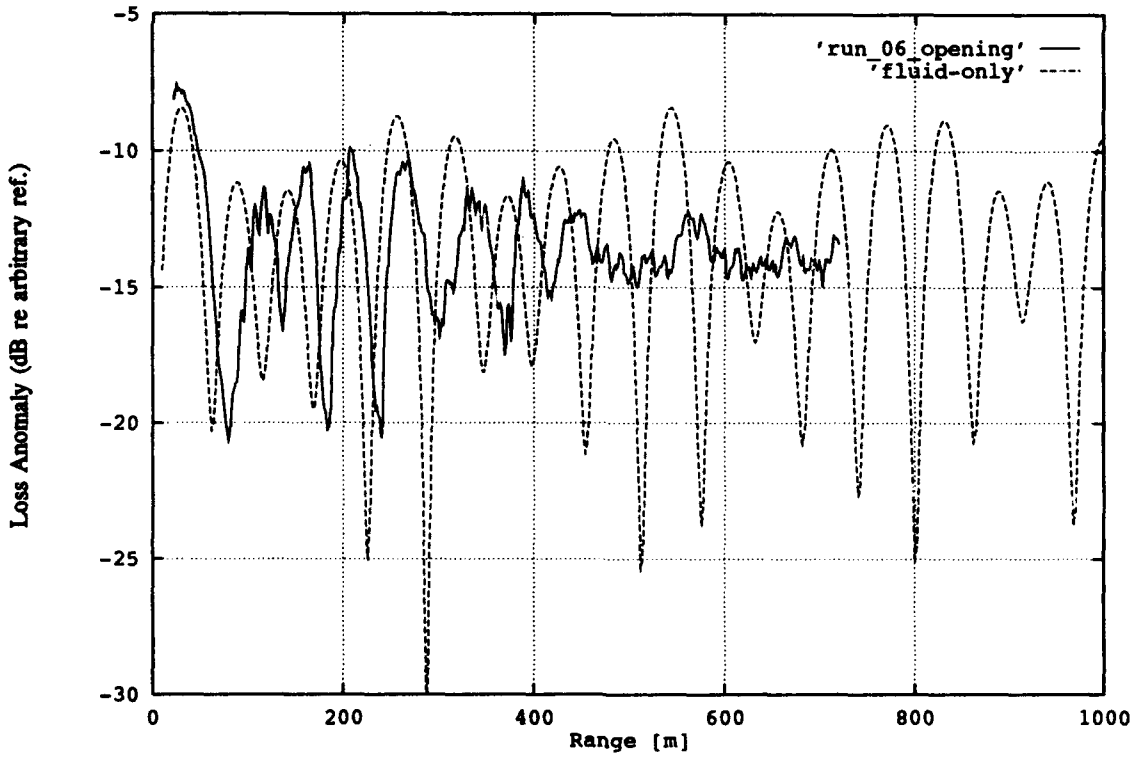

(b)

Fig. 8 — Comparison of measured relative CW loss anomaly vs range with the predictions of the fluid model at 80 Hz for the (a) closing-range and (b) opening-range tracks of run 6 along the 17-m isobath

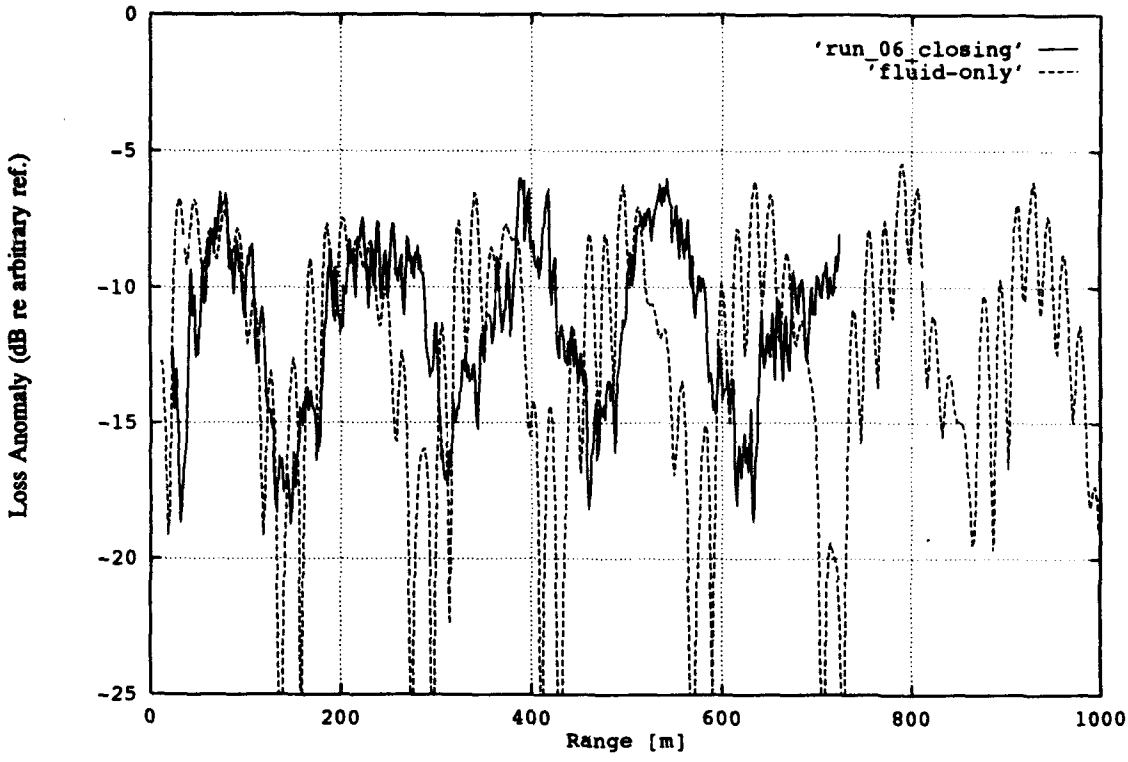

(a)

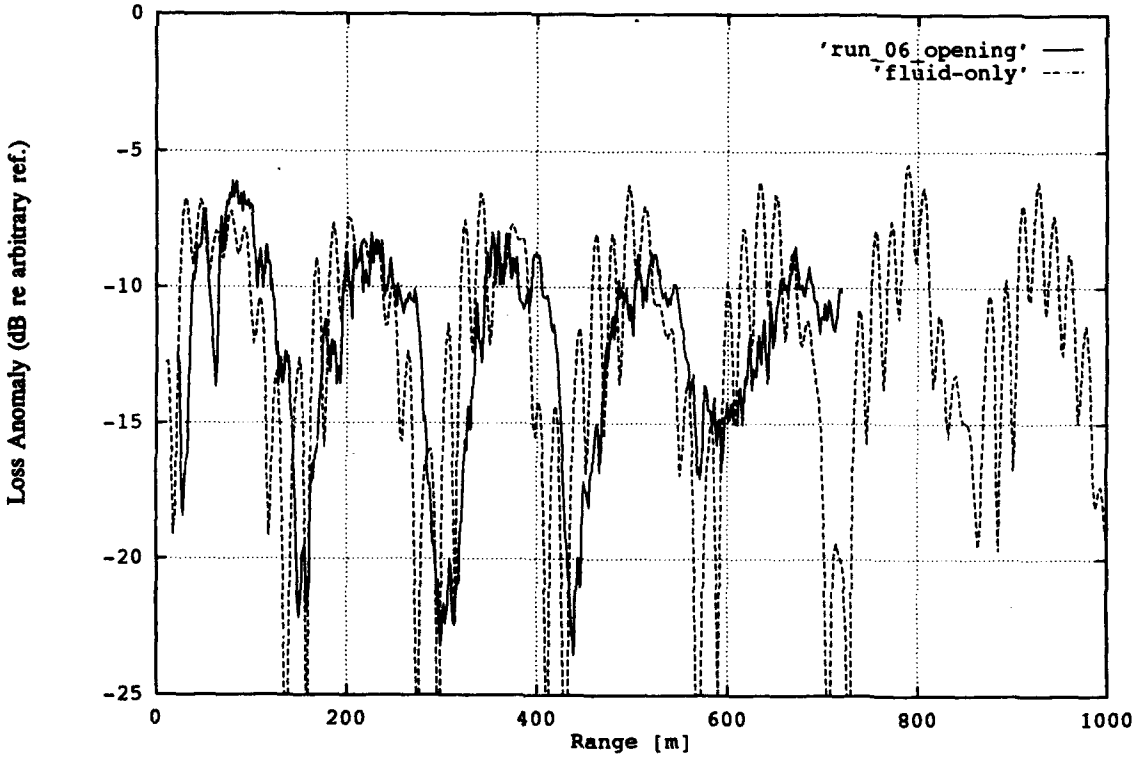

(b)

Fig. 9 — Comparison of measured relative CW loss anomaly vs range with the predictions of the fluid model at 175 Hz for the (a) closing-range and (b) opening-range tracks of run 6 along the 17-m isobath

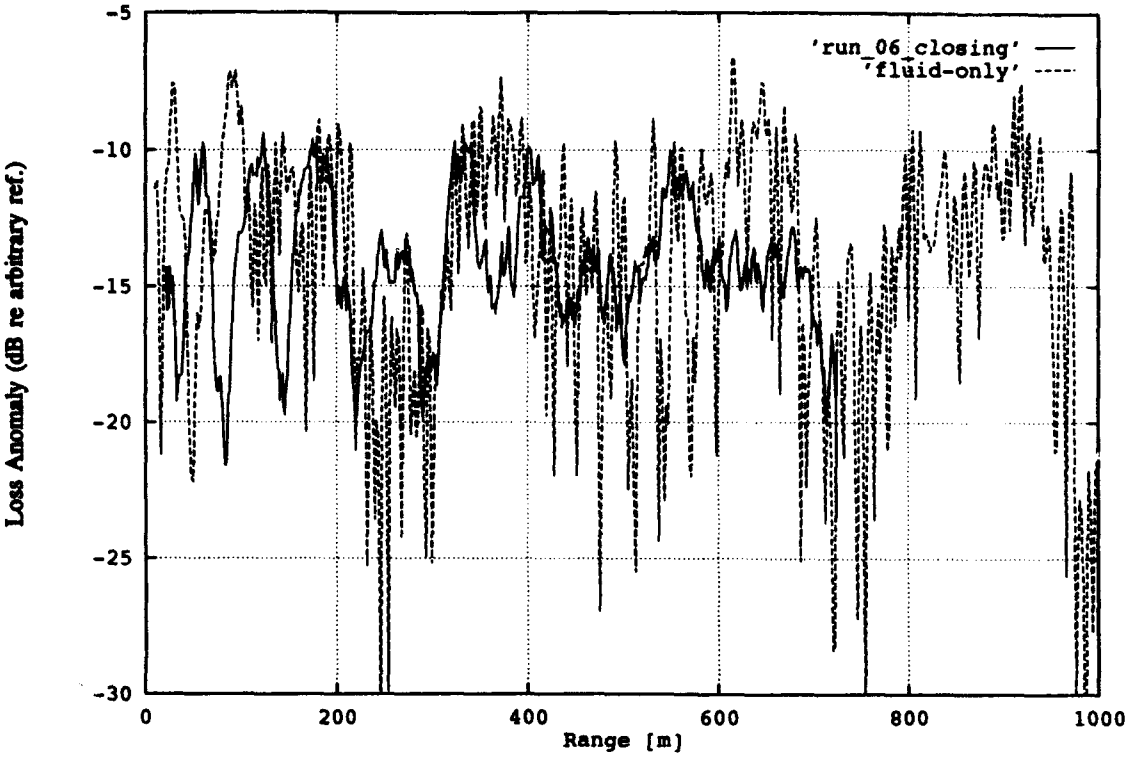

(a)

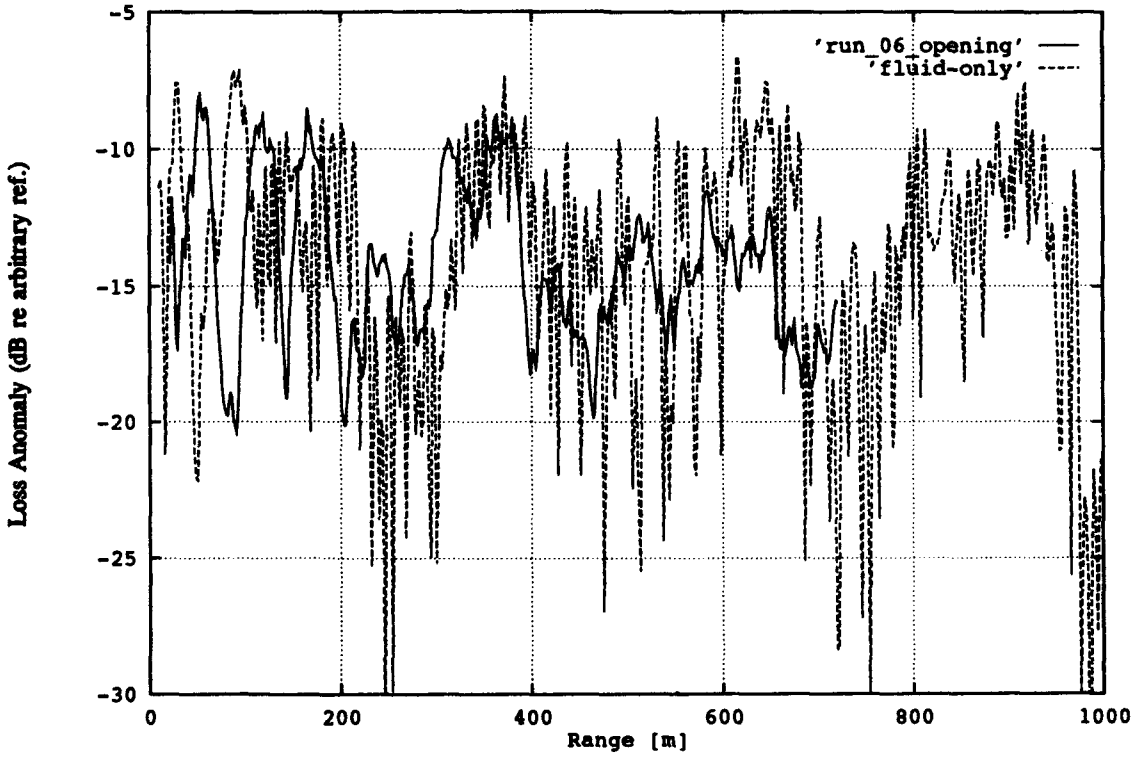

(b)

Fig. 10 — Comparison of measured relative CW loss anomaly vs range with the predictions of the fluid model at 375 Hz for the (a) closing-range and (b) opening-range tracks of run 6 along the 17-m isobath

As we decrease the frequency from 80 Hz, the character of the spatial interference changes. In Fig. 11, we show the data-model comparisons at 50 Hz. While the low spatial frequency oscillation seen in the model results appears to be present in the measurements, a higher frequency interference is present. A similar conclusion can be drawn from the 24 Hz results shown in Fig. 12. The low spatial frequency trends in the model results are seen in the data, and the amplitude of the low-frequency oscillation in both the model results and the data is larger than that observed at 50 Hz. Figure 13 shows comparison of the lowest frequency (12 Hz) model-data results. The very low-frequency oscillation in the loss anomaly calculated from the fluid model has a period of about 1000 m. The measurements show a suggestion of such a trend, but the interference pattern is dominated by a higher frequency oscillation that has a spatially periodic component of period about 30 m. This high spatial frequency feature was a reproducible experimental result, as was discussed above in Section 5.1. We were unable to obtain the required wave number differences (about 0.03 m^{-1}) among any normal-mode pair with reasonable values of the environmental parameters by using a fluid normal-mode model. As the frequency is reduced from 80 Hz (Fig. 8) to 50 Hz (Fig. 11) we observe a departure of the spatial interference frequency from the usually observed trend in which the spatial frequency increases with harmonic frequency. This departure suggests a change in the physical mechanisms controlling propagation phenomena. The most probable explanation for this difference is the generation of shear waves in the sediment, a phenomenon not treated by the fluid model. We ran a few test cases with the KRAKEN normal-mode model [6], which does permit the inclusion of shear effects. Figure 14 shows the results obtained at 12 Hz by using an assumed shear speed in the sand of 250 m/s. Other parameters used in this calculation were H_2 = 70 m, C_{2P} (H_1) = 1632 m/s, C_{2P} (H_1 + H_2) = 1642 m/s, C_{3P} = 4000 m/s, and C_{3S} = 2000 m/s.

Spatial interferences which have a spatial structure similar to those observed are seen in the shear-model results. From this agreement we conclude that an explanation of the high spatial frequencies observed in the 12, 24, and 50 Hz data need to consider shear effects. The inclusion of shear effects in modeling transmission phenomena has consequences that are likely to have greater importance in this application than merely that of correctly accounting for the spatial frequencies in the sound field. As discussed in Appendix C, the acoustic modeling allowed us to estimate the source level of the uncalibrated sound sources from the calibrated signal data. By using the fluid model results, the source level estimated for the 12 Hz fundamental emission of the low-frequency source, when operated with a 1/2 in. stroke, was an unrealistic 200 dB re 1 μPa @ 1 m. Inclusion of shear effects reduced the source level estimate to a more reasonable value of 188 dB re 1 μPa @ 1 m. The accurate determination of radiated noise of ships requires an accurate accounting of transmission phenomena. If this accounting is to be performed by using acoustic transmission models, then the correct treatment of environmental influences is of crucial importance.

In the 24 and 12 Hz data (Figs. 12 and 13), we consistently observe an additional feature that was not reproduced in any of the modeling. This feature is a high-intensity signal at ranges less than about 50 m. The normal-mode models used do not incorporate the contributions of the branch-line integral required for a complete normal-mode treatment [1, p. 82]. This nonpropagating term is characterized by purely imaginary wave numbers and is rapidly attenuated as range is increased. We hypothesize that the short-range, high-intensity signal observed may be explained by considering this contribution. Verification of this hypothesis is left for a future investigation.

47-m Water Depth

In general, the fluid model was able to account for most of the features of the loss anomaly observed in propagation along the 47-m isobath. As was the case with the 17-m isobath data, the environmental parameters that best fit the data differed somewhat from frequency to frequency; however, the values that provided the best fit of the deeper water data were found to lie in the same range as those obtained for the data from the 17-m isobath.

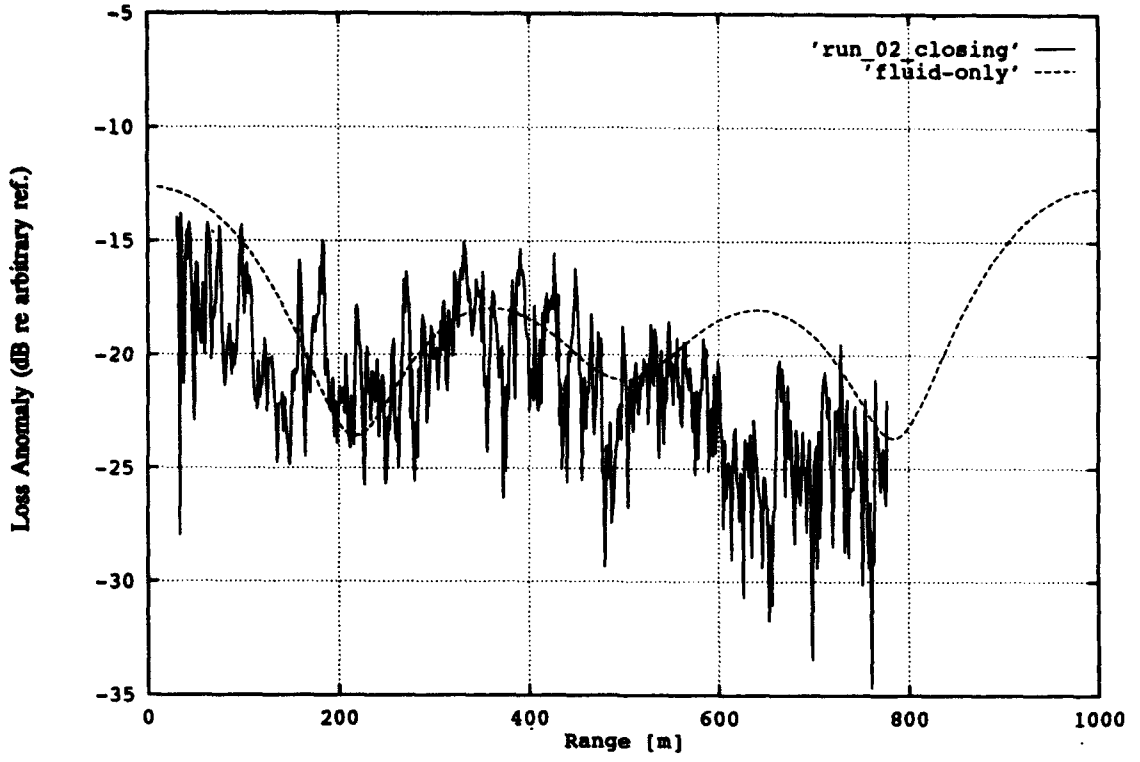

(a)

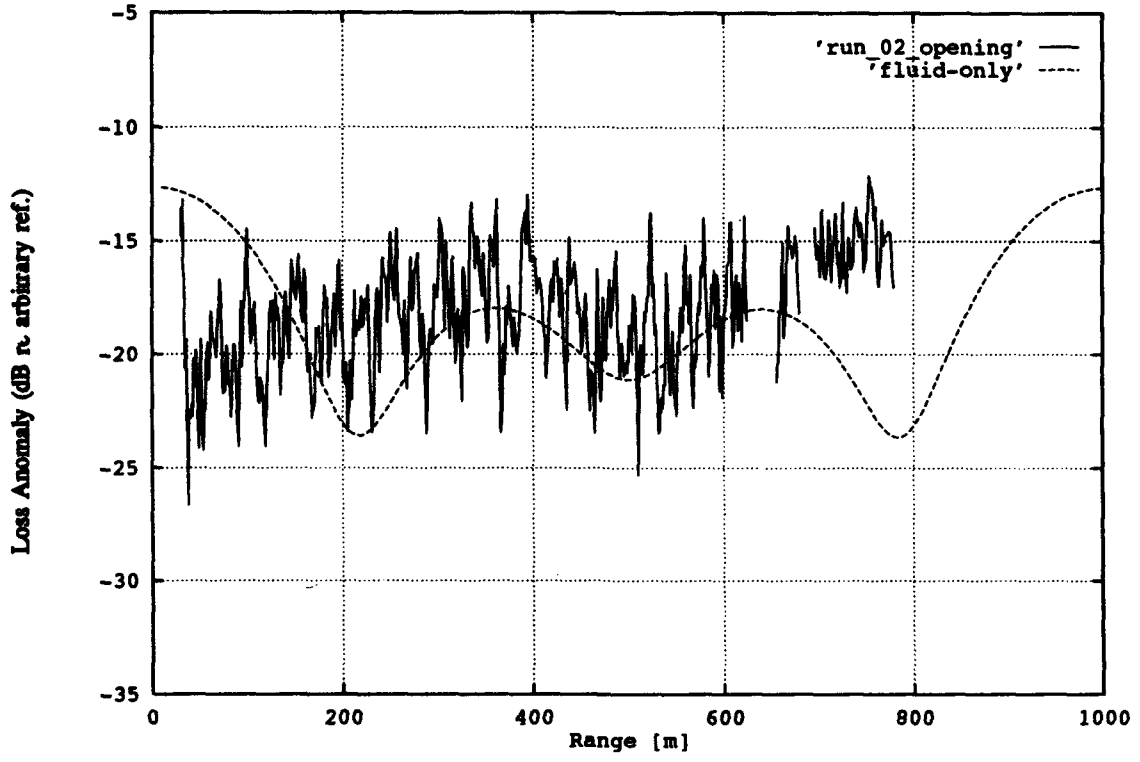

(b)

Fig. 11 — Comparison of measured relative CW loss anomaly vs range with the predictions of the fluid model at 50 Hz for the (a) closing-range and (b) opening-range tracks of run 2 along the 17-m isobath

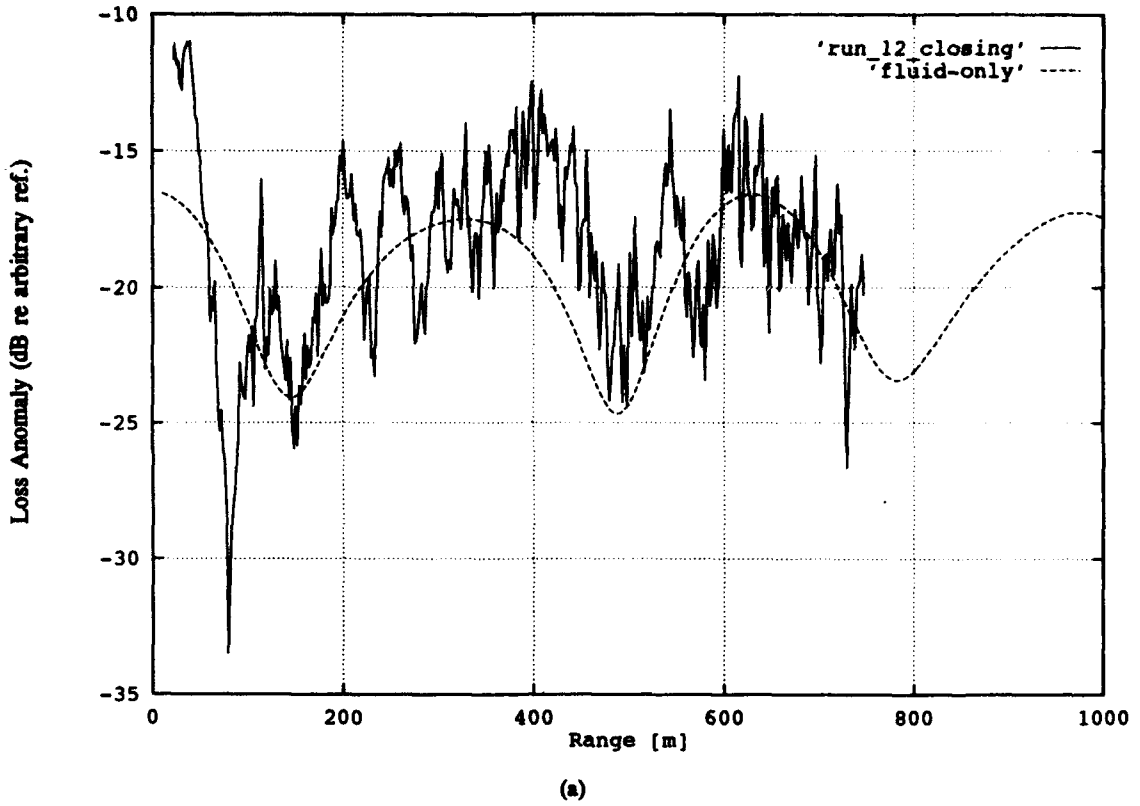

(a)

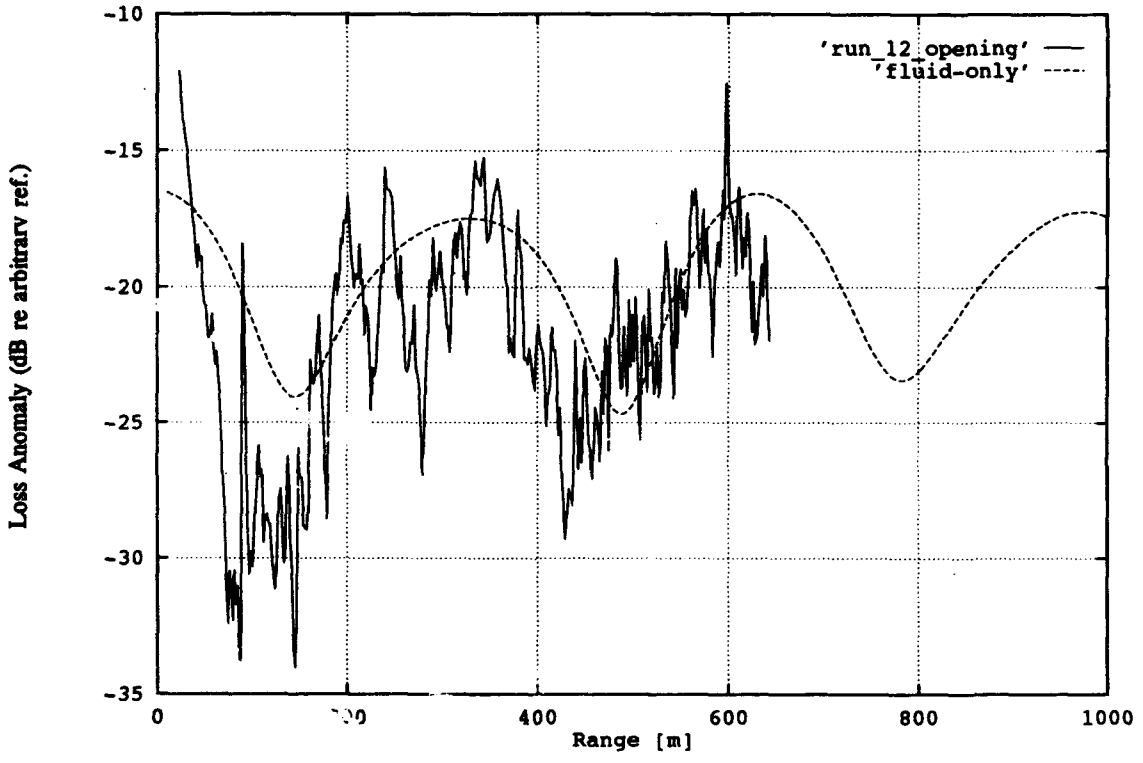

(b)

Fig. 12 — Comparison of measured relative CW loss anomaly vs range with the predictions of the fluid model at 24 Hz for the (a) closing-range and (b) opening-range tracks of run 12 along the 17-m isobath

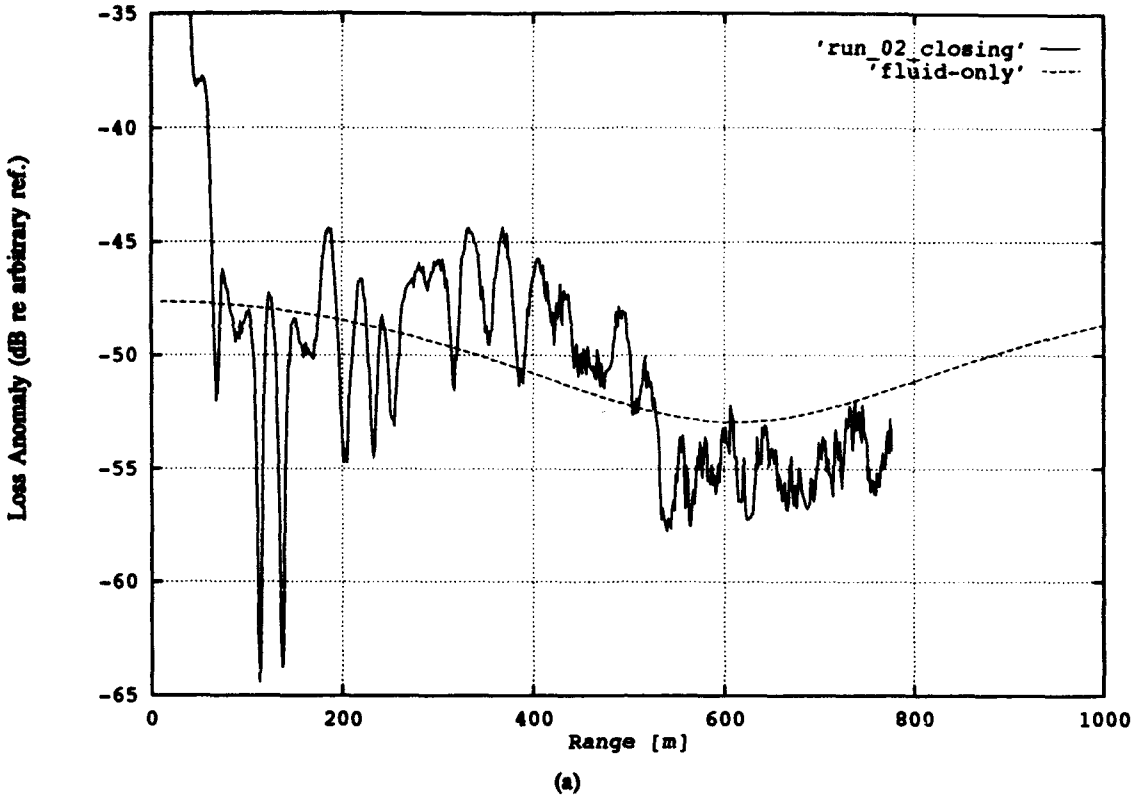

(a)

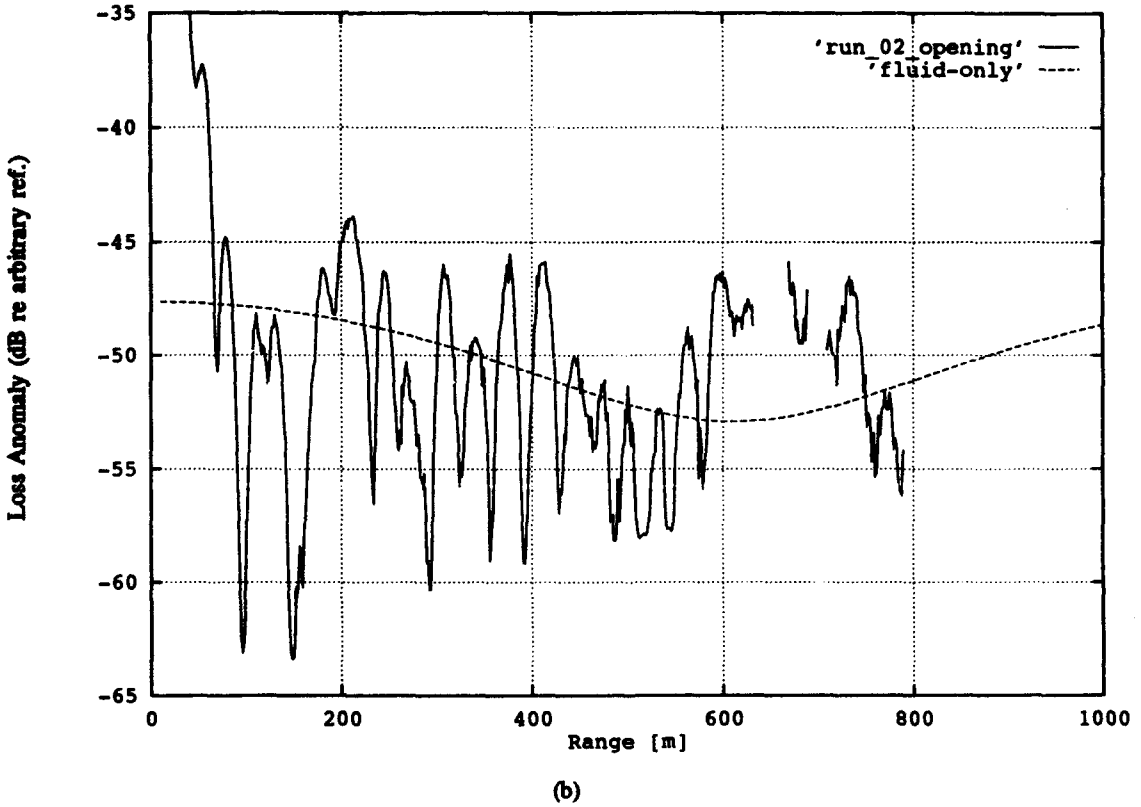

(b)

Fig. 13 — Comparison of measured relative CW loss anomaly vs range with the predictions of the fluid model at 12 Hz for the (a) closing-range and (b) opening-range tracks of run 2 along the 17-m isobath

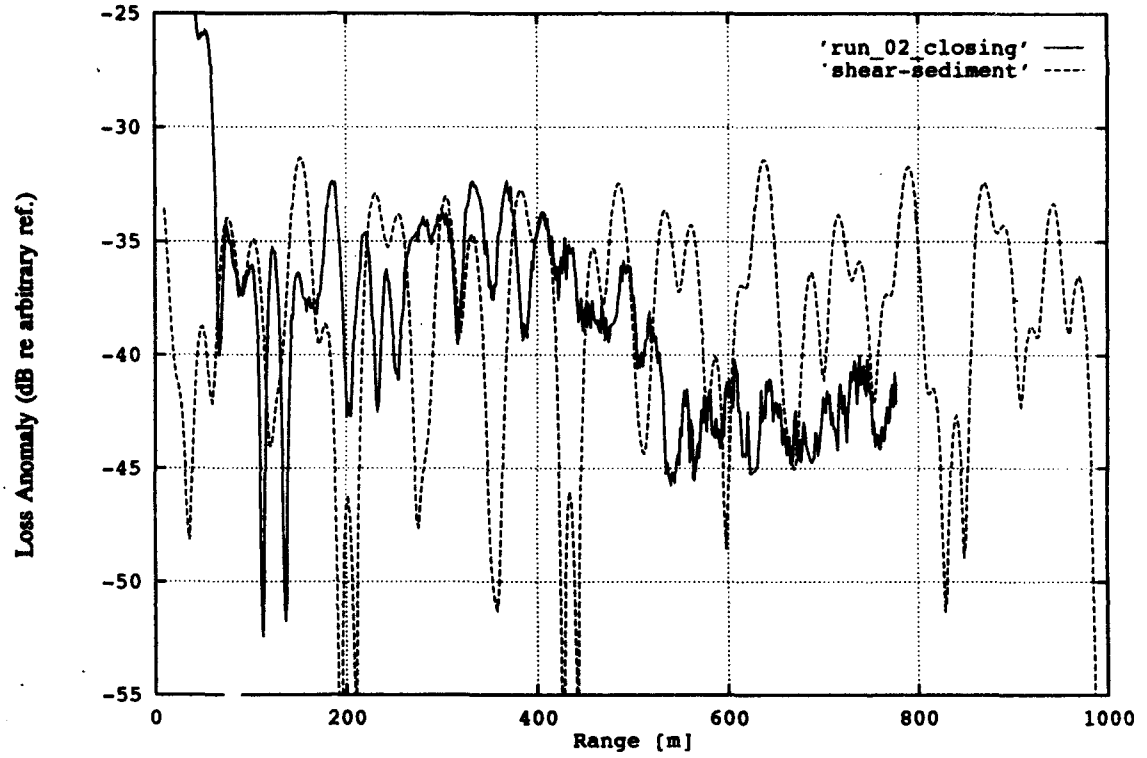

Fig. 14 — Comparison of measured relative CW loss anomaly vs range with the predictions of the shear-supporting model at 12 Hz for the closing-range track of run 2 along the 17-m isobath

Figure 15 shows the results obtained at 12 Hz. In contrast to the shallower water results at this frequency, the fluid model seems to represent the observed loss trends very well. The high spatial frequency oscillations in the signal level observed along the 17-m isobath are absent here. The explanation of the apparent absence of shear effects should be pursued in the follow-on work.

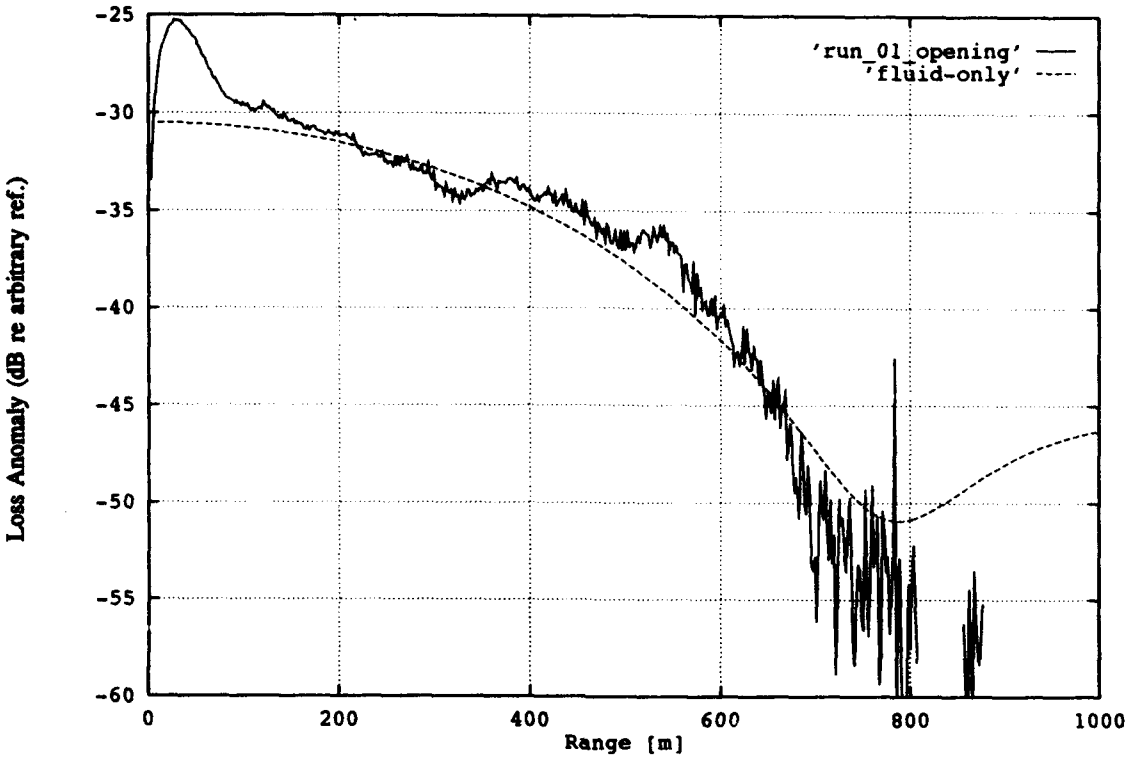

Fig. 15 — Comparison of measured relative CW loss anomaly vs range with the predictions of the fluid model at 12 Hz for the opening-range track or run 1 along the 47-m isobath

The principal features of the 24 Hz signal oscillations were reproduced in the fluid model calculations (Fig. 16). There appears to be some high spatial frequency contributions, possibly those of shear waves. The 50 Hz data shown in Fig. 17 likewise have an interference dominated by higher spatial frequency terms than are reproduced in the calculations. At 80 Hz (Fig. 18), the model results show closer agreement with the data, particularly with regard to the dominant interference patterns observed.

We found that as the harmonic frequency was increased above 80 Hz, the spatial frequency continued to increase, as expected. On account of the rapid oscillation of signal level with range, judgment of the agreement of measured and calculated transmission was very subjective. Consequently these results are not shown here.

CONCLUSIONS

The results obtained in this work show that the fluid-only model adequately explains the data from the 17-m isobath runs for the frequencies of 80 Hz and above. At frequencies below 80 Hz, the fluid model does not produce the high spatial frequency observed in the data. The inclusion of shear effects seems to be necessary to model the observed spatial fluctuations.

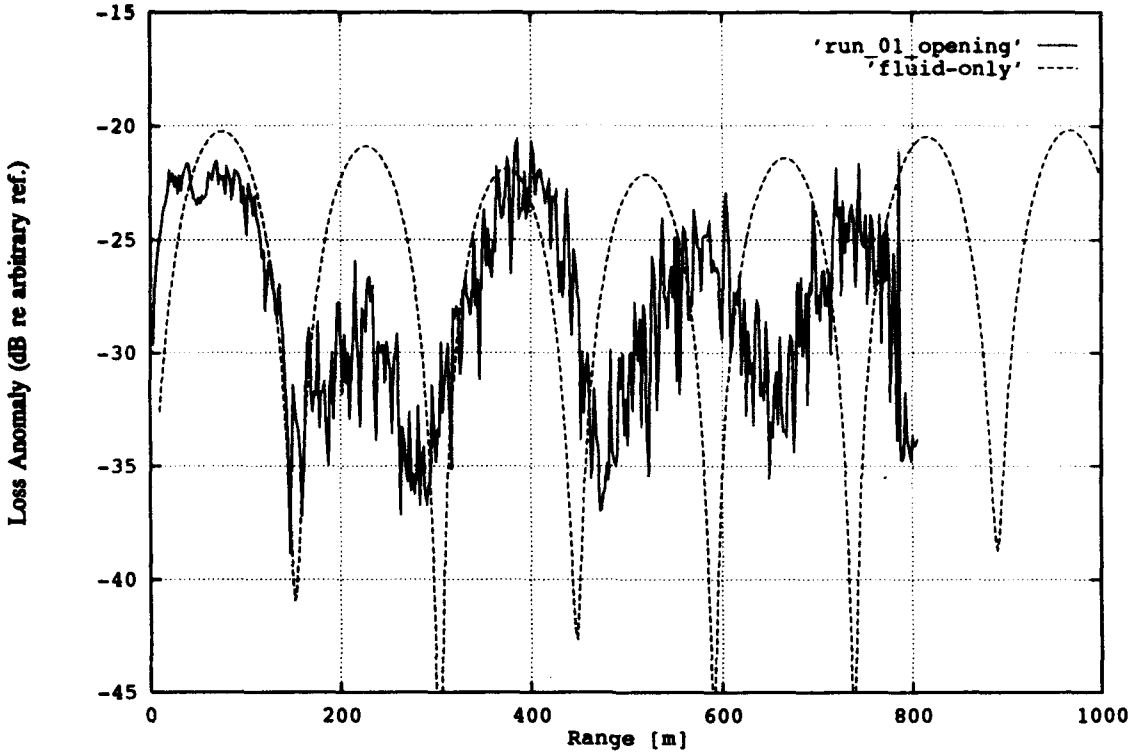

Fig. 16 — Comparison of measured relative CW loss anomaly vs range with the predictions of the fluid model at 24 Hz for the opening-range track of run 1 along the 47-m isobath

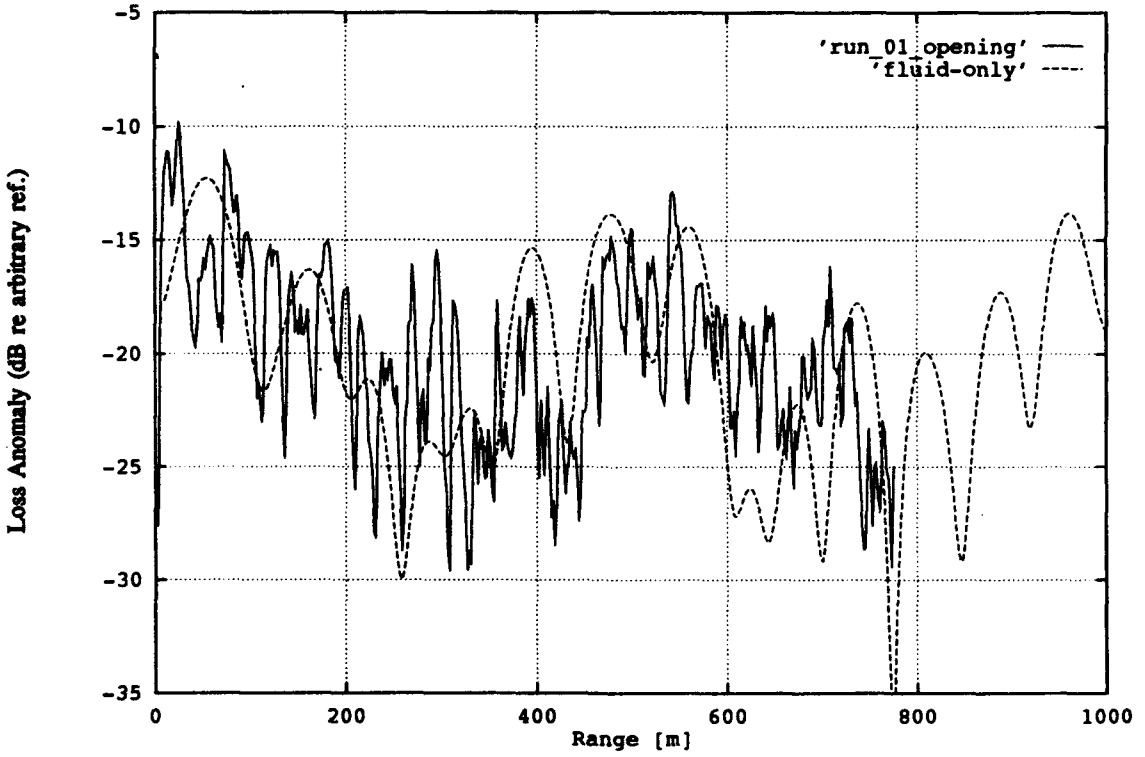

Fig. 17 — Comparison of measured relative CW loss anomaly vs range with the predictions of the fluid model at 50 Hz for the opening-range track of run 1 along the 47-m isobath

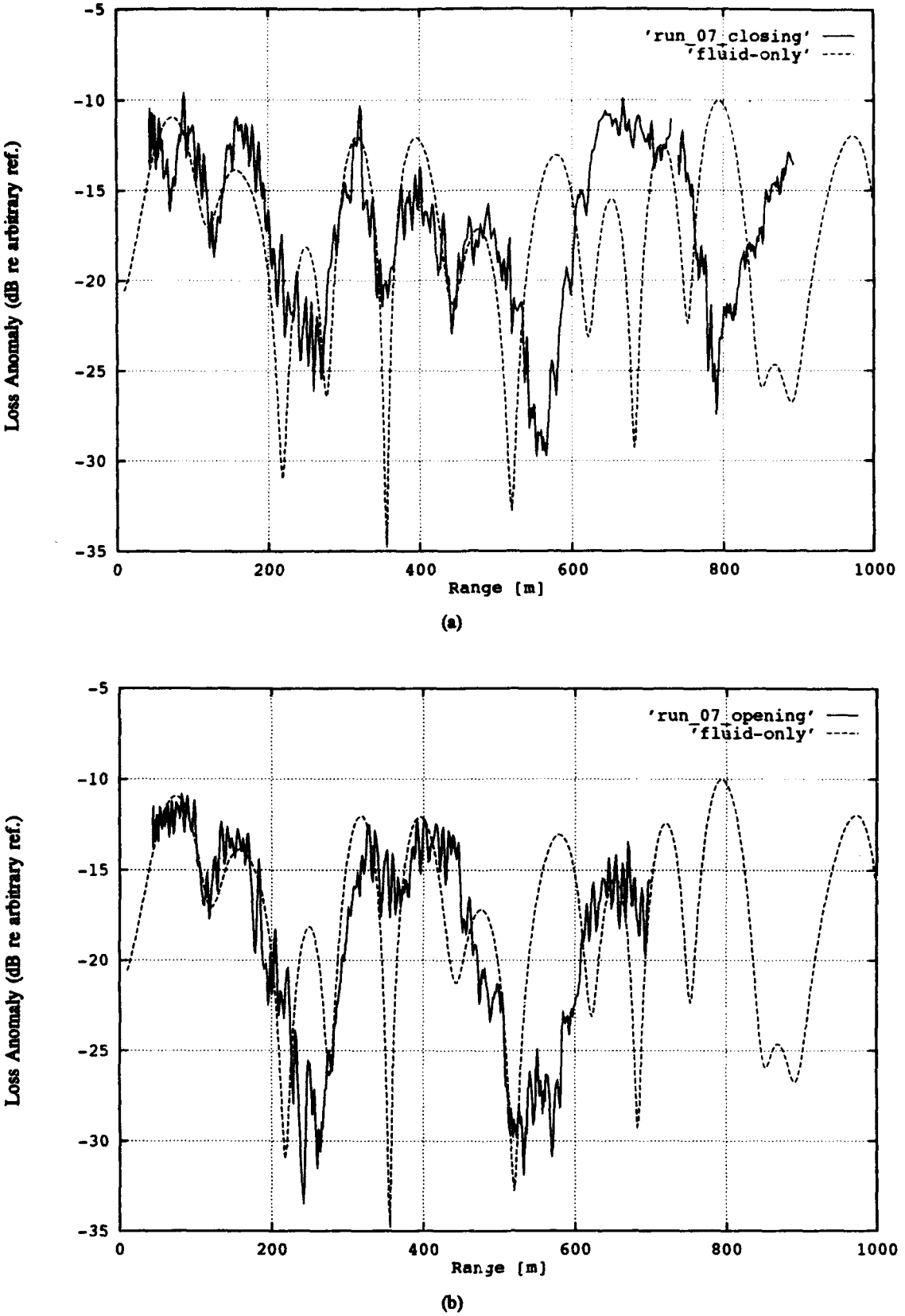

Fig. 18 — *Comparison of measured relative CW loss anomaly vs range with the predictions of the fluid model at 80 Hz for the (a) closing-range and (b) opening-range tracks of run 7 along the 47-m isobath*

The sources used for this work were found to be useful for investigating sound propagation at short ranges. The low-frequency source is most useful at frequencies from 12 to 80 Hz, and the high-frequency source provided good measurements from 80 to 400 Hz. It is necessary to calibrate these sources to obtain their absolute source levels, so the predictions of the absolute values of transmission loss may be tested.

RECOMMENDATIONS FOR FURTHER WORK

The recommendations for further investigations emerging from this preliminary study fall into two categories: (a) work that can be carried out by additional model analyses of the existing recordings and (b) recommendations for experimental improvements to be incorporated into future field work.

For continuing analyses of these data we recommend the following:

- Additional archival sources of information, particularly those concerning the acoustical properties of the ocean sediments and their layering, should be consulted to guide the selection of model parameters .
- The modeling work at the lower frequencies (< 80 Hz) should be pursued to test the preliminary indication that shear waves are generated. Of particular interest is the apparent absence of the shear effects at 12 Hz along the 47-m isobath. A possible explanation for this observation is that the shear modes are confined to the boundary. The modes would then be evanescent in the water column and consequently may not be strongly excited by the source as the water depth increases. Reduction of data for tracks that do not lie along isobaths may be informative since the postulated evanescence of the shear modes in the water column may be more clearly shown along these tracks.
- The apparent frequency dependence of some of the model parameters required for the "best fit" to data suggests that sound speed gradients in the ocean bottom may play an important role. The use of gradients should be explored to attempt to develop a frequency-independent acoustic environment.
- At the higher acoustic frequencies, model-data comparisons carried out by direct examination of the range-dependent interferences were found to be somewhat subjective. Some of the difficulties may be removed by Fourier transforming the loss anomaly in measurements and calculations so the spatial frequencies may be more readily compared.
- The explanation of the high signal-level anomaly at low frequencies and very short (less than 50 m) range, possibly by evaluating the branch-line contributions to the field, is required if very short-range radiated noise measurements are to be interpreted by modeling.

Follow-on field work to "calibrate" the acoustic range should incorporate these improvements:

- Calibration of the sound sources to obtain absolute source levels will permit the testing of the absolute values of loss predicted by the models. This issue is a fundamental one for the use of the range in measuring radiated noise levels of ships.
- For work at the higher frequencies, where refractive effects in the water column will be important, it will be necessary to measure the sound speed profile in the water column concurrently with the conduct of the acoustic measurements. The sound speed profile data should be accompanied by ocean surface wave data, since scattering by surface waves is expected to be important at higher frequencies. Acoustic model runs will be helpful in establishing the acoustic frequency range over which refraction in the water column is important.
- It is likely that some variation in the source level, particularly at harmonics of the fundamental frequency, are present in the current measurements and will be found in future work. A trailing

hydrophone should be installed on the sound sources, and its calibrated signal should be telemetered to the recording station, so simultaneous source level measurements will be available with the received acoustic data. The availability of this data signal would also permit the complex signal pressure to be measured and modern geophysical inversion techniques [7] to be applied to the data to develop more reliable acoustic model inputs.

- The high-quality navigation data available for the existing data set were found to be crucial for the reduction and interpretation of the results. The practice of obtaining high-precision navigation data with the acoustic data should be continued.
- Geophysical work should be performed to obtain the characteristics of the bottom. This work should include core sampling, bottom roughness evaluation, and refraction tests. It is important to define the shear and compressional properties of the bottom, sediment thickness, and range dependence of the parameters.
- In the present work, no attention was paid to the possibility of acoustic reflections from the nearby shoreline. This point should be investigated, possibly by using an impulsive source such as an airgun, to ensure that the energy in such reflected paths is sufficiently small that it may safely be neglected in measurement and modeling.

ACKNOWLEDGMENTS

The analysis and modeling work was performed during a visit to the Naval Research Laboratory (NRL) by researchers from IPqM (Brazilian Navy Research Institute). Support for this visit was provided by the Brazilian Navy. NRL's support was provided by the Office of Naval Research, Code 4530.

At-sea measurements were designed by CASNAV (Naval Systems Analysis Center) and performed by IPqM.

REFERENCES

1. I. Tolstoy and C. S. Clay, "Ocean Acoustics: Theory and Experiment in Underwater Sound," *Acoustical Society of America* (1987).
2. R. W. Hasse, R. L. Martin, and C. E. Parente Ribeiro, "Jaguar-Brazil - Joint U.S./Brazil Acoustic Experiment Exercise," NUSC Technical Report 5543, 1977.
3. *Oceanographic Chart 1500, Brazilian Directorate of Hydrography and Navigation*, 2nd ed., October 1963 (also published as *Chart 24160* by the Defense Mapping Agency Hydrographic Center, 17th ed., May 1978).
4. J. F. Miller and S. N. Wolf, "Modal Acoustic Transmission Loss (MOATL): A Transmission-Loss Computer Program Using a Normal-Mode Model of the Acoustic Field in the Ocean," NRL Report 8429, Aug. 1980.
5. J. F. Miller and F. Ingenito, "Normal Mode FORTRAN Programs for Calculating Sound Propagation in the Ocean," NRL Memorandum Report 3071, June 1975.
6. M. B. Porter, "The KRAKEN Normal Mode Program," SACLANTCEN Report MR-SM-245, Sept. 1991 (also published as NRL Report NRL/MR/5120-92-6920, May 1992).
7. S. D. Rajan, G. F. Frisk, and J. F. Lynch, "On the Determination of Modal Attenuation Coefficients and Compressional Wave Attenuation Profiles in a Range-Dependent Environment in Nantucket Sound," *IEEE J. Ocean Engineering*, **17**(1), 118-128 (1992), and the references contained therein.

Appendix A
ACOUSTIC SOURCES

Two types of sources were used. Each had a controllable, variable-speed, electric motor coupled to an eccentric drive. In the low-frequency source, an eccentric drive moves two rigid plates back and forth, harmonically displacing a certain volume of water, with the volume depending on the eccentric position in the pulley and on the plate diameter (Fig. A1). The acoustic pressure generated by this source follows the piston motion and is essentially a distorted sinusoid (Fig. A2(a)) with a strong fundamental component at the motor rotational frequency and some weaker harmonics (Fig. A2(b)). The motor rotation can be varied from 700 rpm (~ 12.5 Hz) up to 1200 rpm (20 Hz) with a 1/2 in. (zero-to-peak) piston stroke or up to 1800 rpm (30 Hz) with an 1/8 in. stroke. Because volume displacement is fixed by the stroke value, the acoustic source level of the fundamental component increases with drive frequency.

In the high-frequency source, an eccentric cam drives a piston via a spring. In front of the piston there is a diaphragm, whose edges cannot vibrate. At low motor speed, the piston does not touch the diaphragm; but when the speed is increased, the piston makes longer courses until it strikes the diaphragm face, thus making it vibrate at its natural frequencies (Fig. A3).

The time-domain signal generated by this source (Fig. A4(a)) is the response to an impulse when the piston strikes the diaphragm. In the frequency domain (Fig. A4(b)) we will see a peak at the striking frequency and its harmonics. Figure 4(b) shows this spectrum as a solid line. The levels of the individual lines are modulated by the frequency response of the diaphragm that controls the envelope of the spectrum (dotted line in Fig. A4(b)). Therefore, the highest levels occur near the diaphragm natural frequencies (near 70, 180, and 380 Hz).

Figure A4(c) schematically shows the acoustic source level at the fundamental frequency vs the motor rotational speed. The source level of this acoustic source is low if the drive amplitude, which increases with rotational speed of the motor, is insufficient for the piston to strike the diaphragm. As the drive amplitude (or frequency) is increased, the source level jumps when the piston starts striking the diaphragm (point 1 in Fig. A4(c)). As we increase the drive frequency further, the source level will continue to increase until we reach the frequency at which the piston motion is in resonance with the diaphragm movement (point 2). At still higher motor speeds, the source level is reduced because the piston is in antiresonance with the diaphragm movement. Normally, point 1 is between 900 and 1000 rpm and point 2 between 1400 and 1500 rpm. The source is used in the range where the radiated source level varies nearly linearly with the motor speed—normally from 1200 to 1400 rpm.

These sources produce acoustic radiations whose spectra are rich in harmonics. These acoustic signals were used to acquire CW transmission data simultaneously at a number of frequencies spanning a broad frequency range.

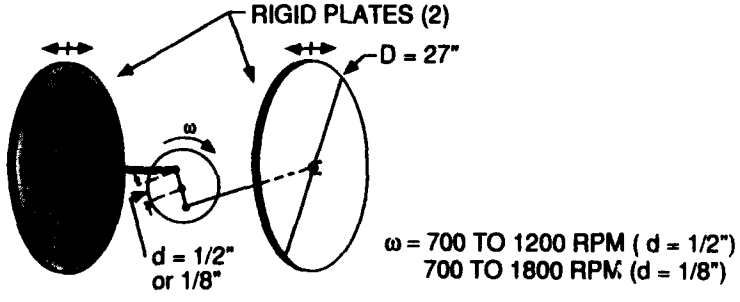

Fig. A1 — Schematic diagram showing operation of the low frequency projector

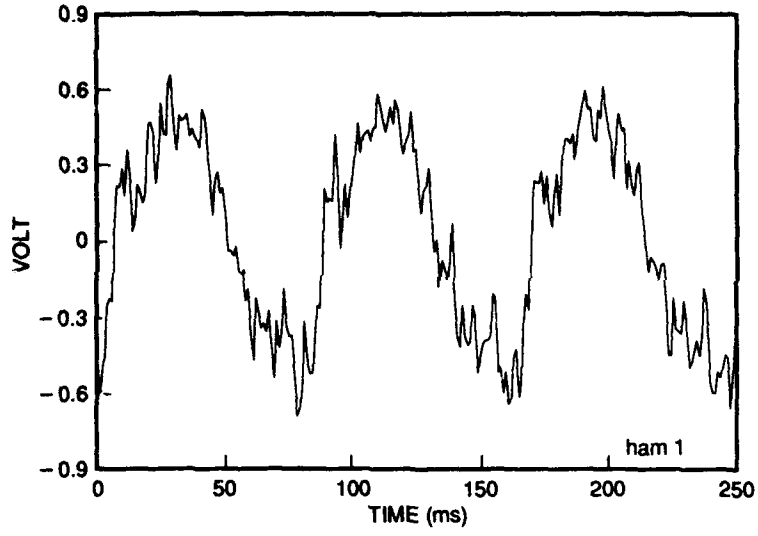

(a)

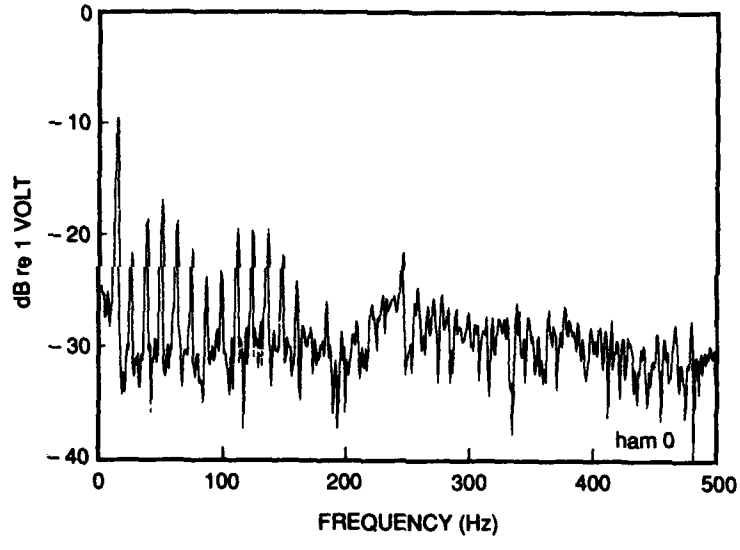

(b)

Fig. A2 — (a) Typical pressure waveform generated by the low-frequency acoustic projector (b) Frequency spectrum of typical signal generated by the low-frequency projector

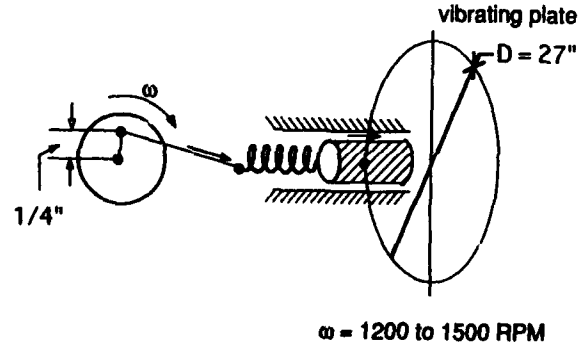

Fig. A3 — Schematic diagram showing operation of the high-frequency (vibrating plate) projector

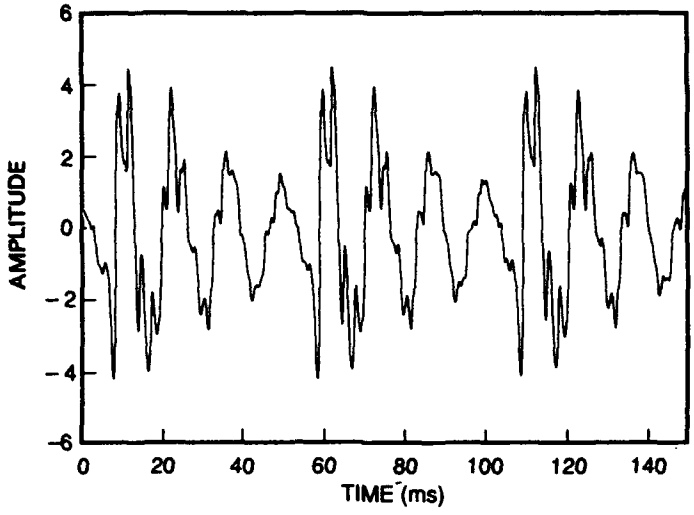

(a)

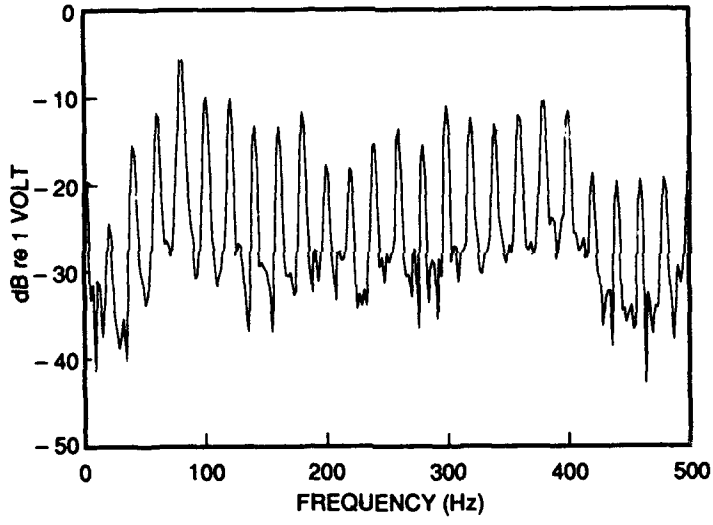

(b)

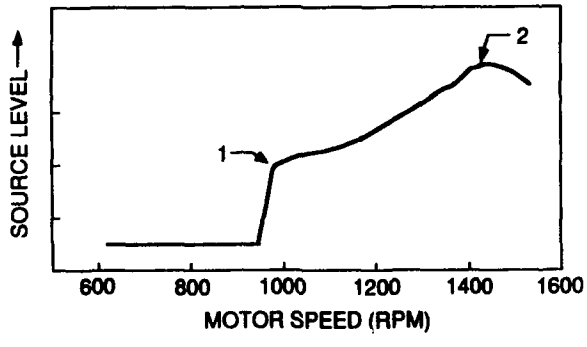

(c)

Fig. A4 — (a) Typical pressure waveform generated by the high-frequency acoustic projector (b) Frequency spectrum of typical signal generated by the high-frequency acoustic projector (c) Dependence of source level of the high-frequency acoustic projector on drive frequency

Appendix B
DATA REDUCTION

Acoustic Data Reduction

Figure B1 shows how the signal recordings were analyzed. A marker cursor on a Fast Fourier transform- (FFT) based spectrum analyzer (Nicolet Scientific Corporation, Model 446A) is used to select the frequency of the level to be studied. When the cursor is positioned on a line of interest the analyzer tracks the measured level by supplying a voltage proportional to the level (in dB re 1 V) at a connector at the rear panel of the analyzer. This voltage was then sampled and digitized by an analog-to-digital converter installed in a personal computer. The initial sampling rate used for the spectrum analyzer's output was 20 Hz. This sample series was 10-point-smoothed (linear average) to reduce fluctuations observed in the data and then downsampled to 2 Hz. The purpose of using this arrangement was to supply a series of measurements of acoustic level closely spaced in time (and therefore source-receiver range) so that the signal level spatial fluctuations having spatial spectral components on the order .03 m^{-1} could be examined. The time code on the tape was used to synchronize the acquisition. Note that in some cases (particularly with the higher frequency sound source) a small frequency instability was observed, and it was necessary to increase the analysis bandwidth to ensure that the signal line remained in the analysis band. Table B1 gives the source type, the motor rotational speed, the frequencies selected for measurement, and the analysis bandwidth used for each run. This table also gives the spatial sampling corresponding to the temporal sampling rate (as inferred from the tow speed) used.

The signal levels were corrected to absolute pressure at the hydrophone by taking into account the hydrophone sensitivity, any gain used in the recording, and the correspondence between the levels read by the analyzer cursor and the voltage digitized, by using the formula

$$P = Va - G - S, \tag{B1}$$

where P is pressure at the hydrophone in dB re 1 μ Pa; V is voltage digitized from the analyzer rear connector in V; a is a conversion factor to the level read by the cursor in dB/V; G is total gain used in the recording and replay in dB; and S is hydrophone sensitivity in dB re 1 V/μ Pa.

Reduction of Navigation Data

The raw navigation data were reduced to calculate the closest point of approach (CPA) to the hydrophone and to obtain range from the hydrophone vs time. When the navigation data were merged with the acoustic-pressure-vs-time data, it was found that there was a slight asymmetry in the level-vs-range data on the inbound and outbound tow tracks. The source of the asymmetry was considered to be a navigation error. The navigation data were therefore adjusted by offsetting them by a slight amount (up to 20 m) to provide symmetry in the level-vs-range data. Since the source projected several frequencies simultaneously, the reasonableness of this correction was ascertained by the fact that the same navigation offset provided symmetry in the level-vs-range data over a broad frequency range.

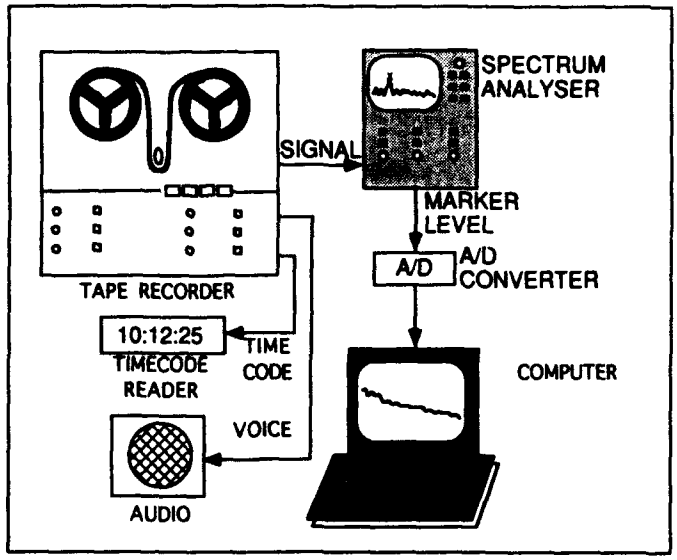

Fig. B1 — Signal analysis equipment

Table B1 — Data Reduction Information

Run #	Water Depth (m)	Source Type	Motor Speed (rpm)	Frequency (Hz)	Bandwidth (Hz)	Spatial Resolution (m)
01	47	Low Freq.	745	12	3.75	1.78
01	47	Low Freq.	745	24	3.75	1.78
01	47	Low Freq.	745	50	7.50	1.78
02	17	Low Freq.	720	12	3.75	1.39
02	17	Low Freq.	720	50	3.75	1.39
06	17	High Freq.	1200-1272	80	7.50	1.28
06	17	High Freq.	1200-1272	175	18.75	1.28
06	17	High Freq.	1200-1272	375	37.50	1.28
07	47	High Freq.	1200-1272	75	3.75	1.44
07	47	High Freq.	1200-1272	375	37.50	1.44
12	17	Low Freq.	745	24	3.75	1.78

Appendix C
MODELING

Modeling Procedures

A three-layer environmental model was used for the acoustic range, as shown in Fig. C1. The first layer is the water column, bounded above by the pressure-release surface and below by a sediment layer that can be a fluid or a shear-supporting solid. The model computer code allows the compressional and shear sound speed profiles to be arbitrary functions of depth. The third layer is a higher speed, semi-infinite layer that may also be a fluid or a solid. In this layer, the compressional and shear sound speed values are constant. To describe the environment, the following parameters are needed:

H_1 = First layer (water) depth
H_2 = Second layer (sediment) depth
ρ_1 = Density of the first layer
ρ_2 = Density of the second layer
ρ_3 = Density of the third layer (basement)
$C_{1P}(z)$ = Sound speed profile in the first layer
$C_{2P}(z)$ = Sound speed profile in the second layer
C_{3P} = Compressional wave sound speed in the third layer
$C_{3P}(z)$ = Shear sound speed profile in the second layer
C_{3S} = Shear sound speed profile in the third layer
Z_s = Source depth
Z_r = Receiver depth.

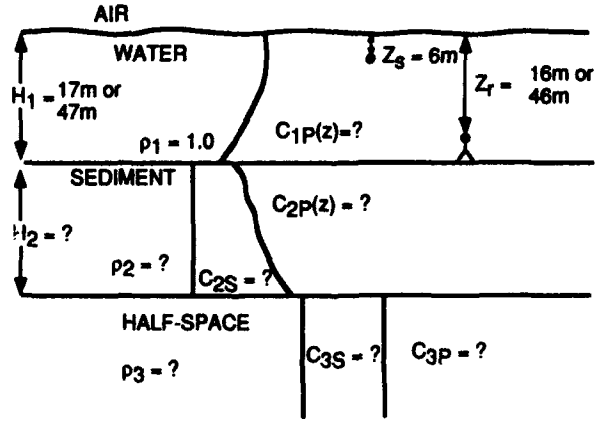

Fig. C1 — The three-layer environment used in modeling

The densities are given relative to the density in water; thus ρ_1 has value 1.0. The shear sound speed parameters are used only if the second and third layer support shear waves.

In this report, only the values $\rho_1 = 1.0$, $H_1 = 17$ or 47 m, $Z_s = 6$ m, and $Z_r = 16$ or 46 m are known. The other parameters were initially approximated by using available descriptions of the sediments and were then refined to improve agreement of the calculated loss anomaly and the experimental data.

The acoustic normal-mode programs FLUID [C1,C2] and KRAKEN [C3] were used to calculate the wave numbers, mode amplitudes, and transmission loss for a given environment. The first program, FLUID, was used when the sediment layer was considered a fluid (no shear waves supported), while the second one, KRAKEN, was used when it was desired to test the importance of shear waves within the bottom.

The procedure used was to make a file containing all environmental information that was used as the input for the programs. The programs generated output files with the horizontal wave numbers of the normal modes along with the corresponding mode amplitudes. From these data and the depth of source and receiver, propagation loss was calculated for distances up to 1000 m from the source to the receiver. Calculated loss was then compared with the corresponding level-vs-range data for that run. Since the sources used were not calibrated with regard to source level, the received level was offset "by eye" as needed to provide the best agreement with calculated loss. The value of the offset used is an estimate of the source level in dB re 1μPa @ 1 m. Note that when the experiment was conducted, the sources were tested by operating them at different levels in different runs; therefore, the variation of source level from one run to another does not cast doubt on the accuracy of the measurements. Table C1 shows the source level values (i.e. offset) inferred by using this technique.

Table C1 — Source Level Offsets

Run #	Depth (m)	Frequency (Hz)	Offset (dB)
01	47	12	178
01	47	24	150
01	47	50	147
02	17	12	200
02	17	12	*188
02	17	50	150
06	17	80	181
06	17	175	167
06	17	375	175
07	47	75	160
12	17	12	185
12	17	24	147

Note: Offset (dB re 1 μ Pa @ 1 m) added to the experimental data levels to obtain agreement with the calculated loss.
*Offset needed with a shear-sediment model.

Model Sensitivity to Environmental Parameters

The modeling work started by varying the unknown parameters and using the program FLUID to calculate the wave numbers and mode amplitudes. From these values, transmission loss was calculated for the known source and receiver depths, and it was adjusted to remove the 10 log R trend of cylindrical spreading; the resulting quantity is referred to as "transmission loss anomaly." A number of computer runs were made to gauge the sensitivity of the model calculations to ranges of values of the unknown environmental parameters to guide efforts in modeling the data. Before showing some representative runs illustrating the model sensitivity, we discuss the physical reasons behind the sensitivity of the model to the parameters used.

Analytic representations of normal-mode theory show that the normal-mode wave number spectrum consists of two parts—a discrete spectrum and a continuous spectrum. For a simple two-fluid model in which a fluid of sound speed C_{1P} overlays a fluid of higher sound speed C_{2P}, the discrete modes have wave numbers in the range ω/C_{2P} to ω/C_{1P}, and the continuous modes have wave numbers less then ω/C_{2P}. Generally, modeling of long-range propagation can safely neglect the contributions of the

continuous mode spectrum, because these modes interact strongly with the bottom and are rapidly attenuated with range. For the modeling work considered here, propagation to short ranges from the source is of interest, and the modes that interact strongly with the bottom may make important contributions. Further, since the spatial interferences are of particular interest in this study, the range of modal wave numbers included in the calculation is important. The models used in this study calculate only the discrete modal spectrum. To use these models to represent the normal modes that interact strongly with the bottom and to introduce low values of the horizontal wave number, we represent the sand sediment as a layer that overlays a halfspace having higher sound speed C_{3P}. For this environment, the range of wave numbers associated with the discrete modal spectrum extends to lower values bounded by ω/C_{3P}. The number of modes in the wave number interval ω/C_{3P} to ω/C_{2P} is controlled by the thickness H_2 of the sediment layer. As H_2 is increased, more discrete mode orders are allowed, and the wave number interval is more densely populated with discrete modal wave numbers. Other environmental parameters, such as the sediment and halfspace densities, have only a slight influence on the modal wave numbers, with the result that varying these parameters does not strongly influence the calculated interference pattern.

Figures C2 and C3 illustrate respectively the insensitivity of the interference pattern to halfspace and sediment densities. In Fig. C2, loss anomaly is calculated at 80 Hz for a water depth of 17 m and a sediment layer thickness of 100 m. Sound speed in the sediment layer is assumed to be 1630 m/s, and the sound speed in the halfspace is assumed to be 2750 m/s. The halfspace density assumes values 1.0, 2.0, and 3.0 for the curves shown. Changing the density over this large range introduces only a slight shift in the interference pattern, corresponding to small changes in the modal wave number differences. In all three cases the environment supports nine mode orders.

The influence of changing the density in the sediment layer was also found to be small. In Fig. C3, transmission loss anomaly at 175 Hz is shown for an environment with water depth sediment thickness, sediment sound speed, and halfspace sound speed the same as in the case for Fig. C4. Changing the density of the sediment from 1.0 to 2.0 makes only a small change in the modal interference. In this case, 20 discrete normal modes are allowed. In the rest of the modeling runs carried out, values $\rho_2 = 1.8$ and $\rho_3 = 2.0$ were used.

In Fig. C4, the influence of basement sound speed is examined. Transmission loss anomaly is calculated at 175 Hz for an environment having the same water depth (17 m), sediment thickness (100 m), and sediment sound speed (1630 m/s) as used in Figs. C2 and C3. In this example, the basement sound speed values used and the number of discrete modes allowed were (2000 m/s; 15), (3000 m/s; 21) and (4000 m/s; 23) respectively. We note that the low spatial frequency features and overall level do not change as the halfspace sound speed is varied. Calculations using the higher halfspace sound speed values introduce additional mode orders having significantly different wave numbers than those of the lower order modes, and high spatial frequency interferences are introduced.

The sound speed in the sediment can also have significant influences on the wave number spectrum and consequently on the calculated interference pattern. In Fig. C5 we show transmission loss anomaly calculated at 175 Hz, again using $H_1 = 17$ m, $H_2 = 100$ m, and a halfspace compressional speed, C_{3P}, 2750 m/s. The sediment sound speeds, C_{2P}, and the number of modes calculated were (1500 m/s; 23), (1700 m/s; 19), and (1900 m/s; 16), respectively. Increasing the sediment sound speed reduced the number of modes allowed; the mode orders that "dropped" as the sediment speed increased were those associated with the smallest wave numbers, with the result that the high spatial frequency content of the interference pattern was reduced.

The effect of assumed sediment thickness at very low frequency is illustrated in Fig. C6. Here the frequency has been reduced to 12 Hz, and a comparison is made of three assumed sediment thicknesses—100, 200, and 500 m, for an environment that is otherwise similar to the one used in the examples shown above. The thinnest sediment layer results in only one discrete mode of propagation. As

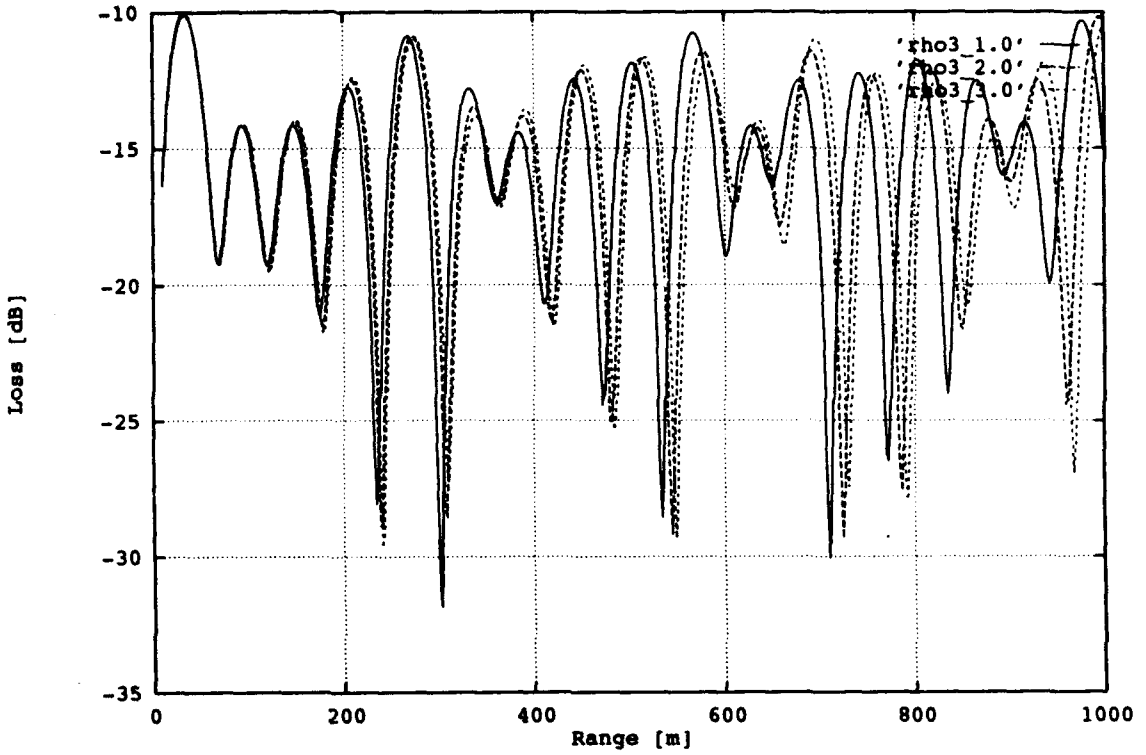

Fig. C2 — Loss anomaly vs range at 80 Hz calculated from the fluid model for three values of density for the halfspace

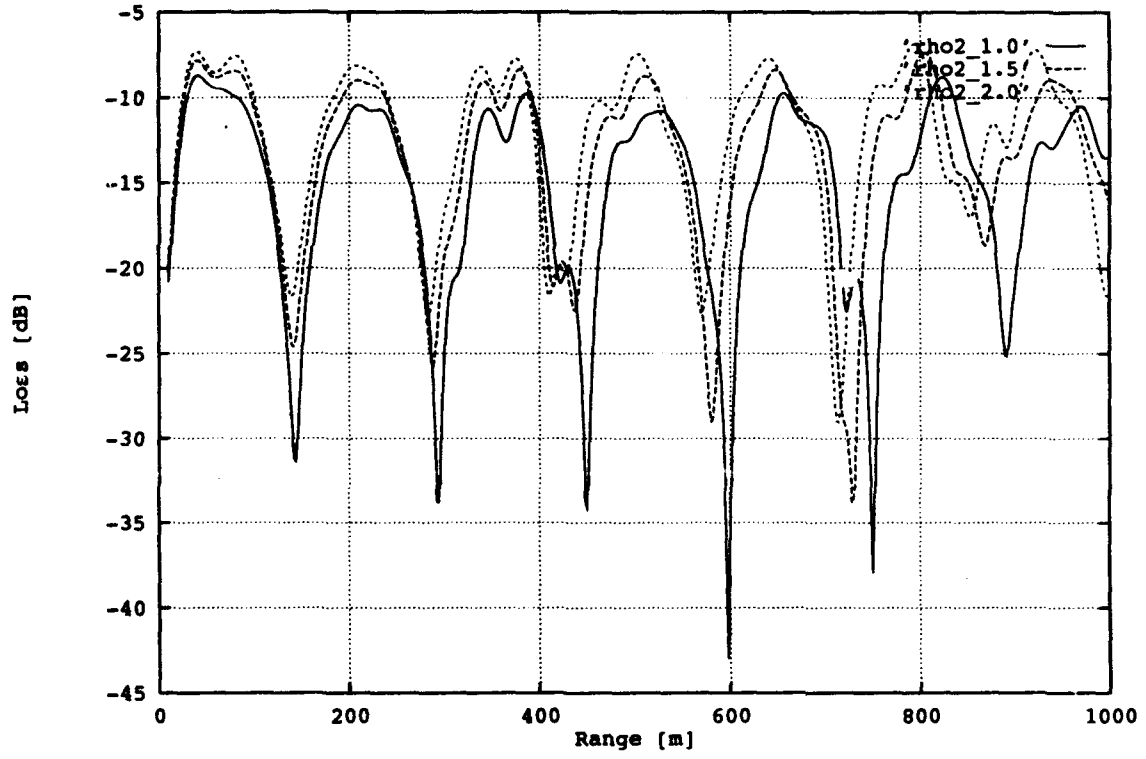

Fig. C3 — Loss anomaly vs range at 175 Hz calculated from the fluid model for three values of density for the sediment layer

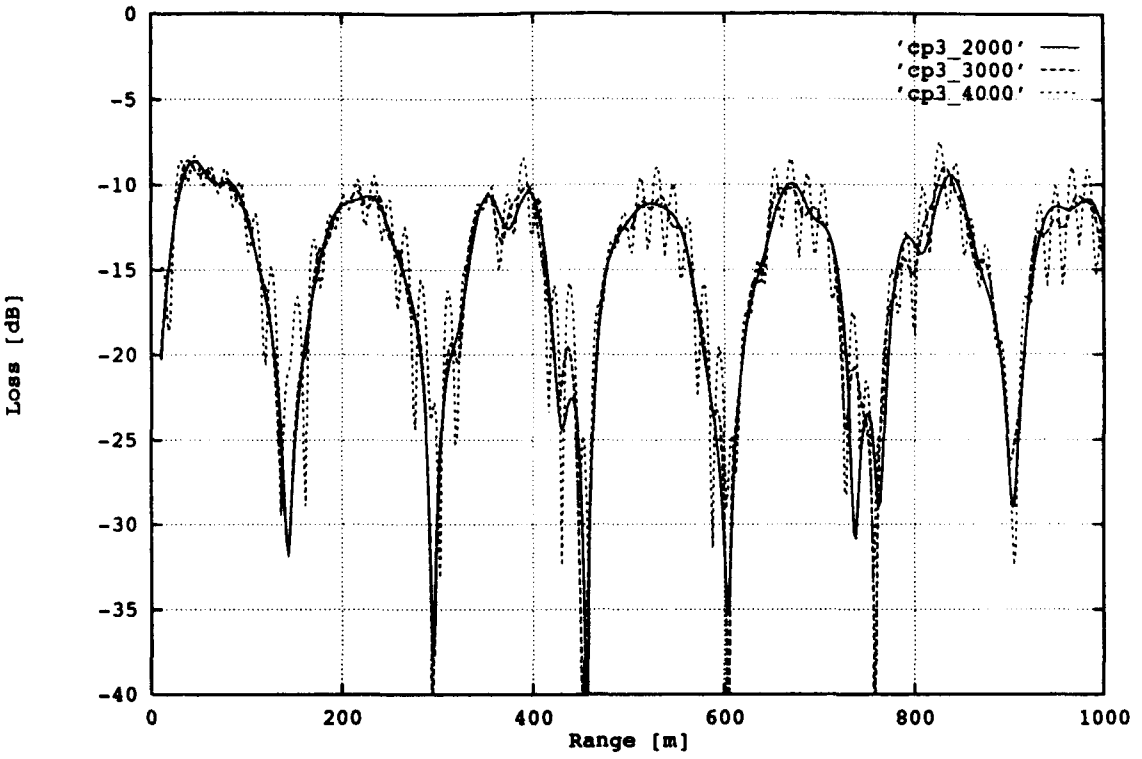

Fig. C4 — Loss anomaly vs range at 175 Hz calculated from the fluid model for three values of the halfspace compressional sound speed

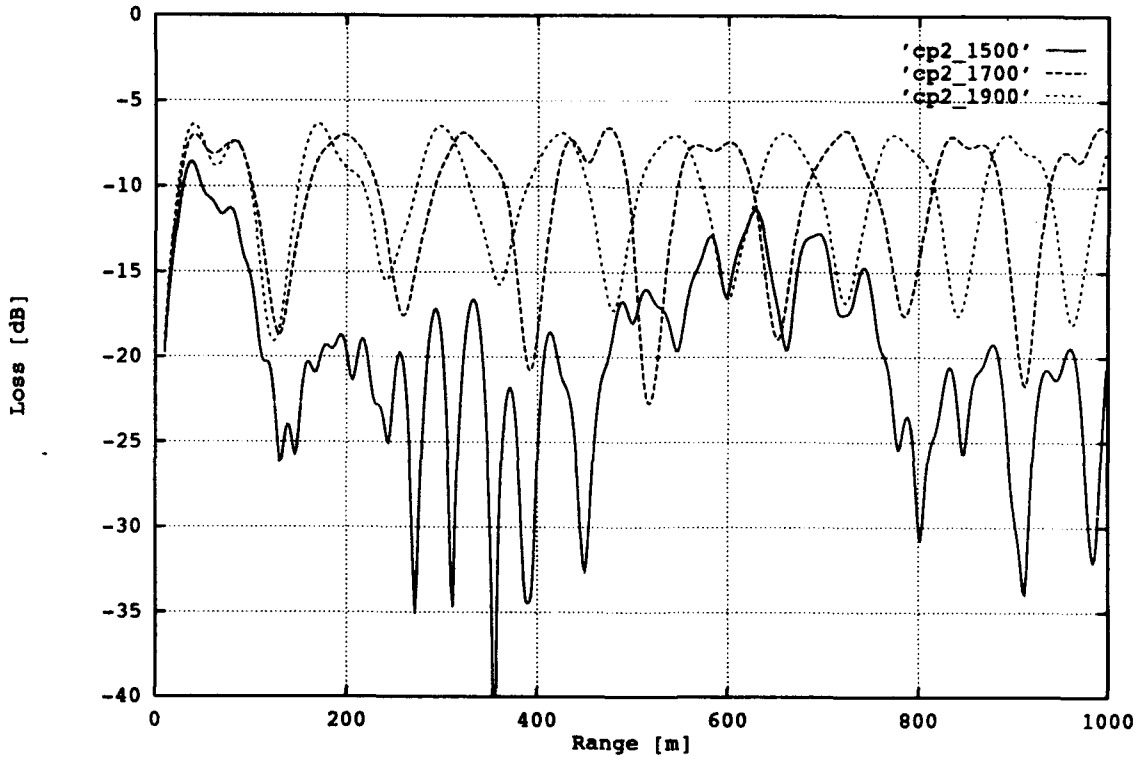

Fig. C5 — Loss anomaly vs range at 175 Hz calculated from the fluid model for three values of the sediment compressional sound speed

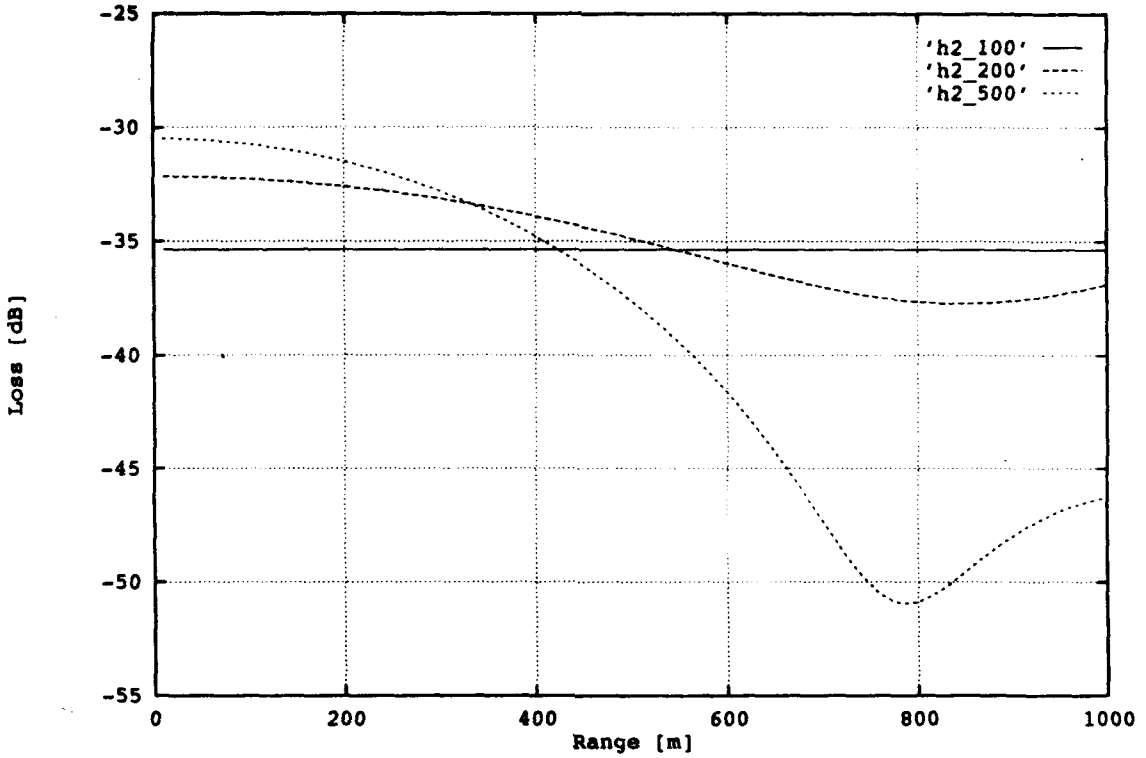

Fig. C6 — Loss anomaly vs range at 12 Hz calculated from the fluid model for three values of sediment thickness

a result, no interferences between mode orders is possible, and the transmission loss anomaly is essentially range independent. When the sediment thickness is increased to 200 m, two mode orders are allowed. When the thickness is further increased to 500 m, five mode orders are allowed, and a deeper interference is seen in this case; however, the spatial frequency content of the interference pattern is not significantly changed. This absence of change may be attributed to the control of the wave number range by the half-space sound speed rather than by the sediment thickness .

Throughout the modeling work an isovelocity sound speed profile was used in the first layer (water column) at 1500 m/s from the surface to bottom.

REFERENCES

C1. J. F. Miller and S. N. Wolf, "Modal Acoustic Transmission Loss (MOATL): A Transmission-Loss Computer Program Using a Normal-Mode Model of the Acoustic Field in the Ocean," NRL Report 8429, August 1980.

C2. J. F. Miller and F. Ingenito, "Normal Mode FORTRAN Programs for Calculating Sound Propagation in the Ocean," NRL Memorandum Report 3071, June 1975.

C3. M. B. Porter, "The KRAKEN Normal Mode Program," SACLANTCEN Report MR-SM-245, Sept. 1991, also published as NRL Report NRL/MR/5120-92-6920, May 1992.